Excited Mercury Complexes

A. B. CALLEAR

Physical Chemistry Department, University of Cambridge, Cambridge CB2 1EP, U.K.

Received February 10, 1986 (Revised Manuscript Received September 23, 1986)

Contents

Reactions of excited mercury atoms have been under investigation for well over half a century. Only quite recently, however, have particular systems of excited complex formation been examined in depth; there now exist several examples for which the fine structure of the kinetics and spectroscopy is revealed in delightful detail. The main object here is to overview what has been achieved in this more recent phase; in addition, tables of rate coefficients are included so that it may be of value as a source of reference.

The material is presented in three parts, first some brief comments on the relaxation of the various atomic states, secondly the formation and luminescence due to mercury dimers and trimers, and finally the formation of excited complexes of mercury atoms with other species.

The style is to define what the author considers to be the status quo in this subject, without belaboring the historic evolution which can be traced from references in the cited publications.

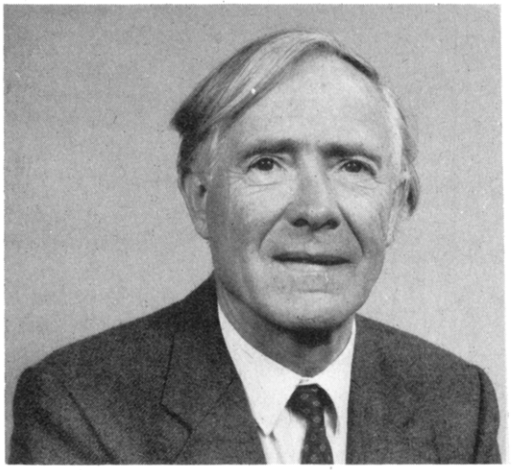

Dr. A. B. Callear obtained his Ph.D. degree at the University of Birmingham, England, in 1954. He spent the following year working with Dr. R. J. Cvetanović at the National Research Council, Ottawa, Canada. During the following 2 years he was employed as a research chemist by Dupont of Canada, at the Research Centre at Kingston, Ontario, Canada. In 1957 he returned to Cambridge, England, to work with R. G. W. Norrish on flash photolysis. He is presently a University Lecturer of Cambridge University and is a Fellow and Tutor at Churchill College. His research interests have largely been within the areas of spectroscopy and kinetics, with a strong emphasis on the excited mercury systems.

I. The Excited Atoms

Some energy levels of the excited mercury atom are shown in Figure 1. Because of spin–orbit coupling in the heavy atom, L and S are not good quantum numbers. The J selection rules hold for optical transitions, $\Delta J = 0 \pm 1$ ($0 \not\leftrightarrow 0$), and also the Laporte rule; even states combine only with odd.

Four states—$^1P_1$, $^3P_2$, $^3P_1$, and $^3P_0$—arise from the 6s6p configuration. Because of the J rules, only lines from $^1P_1$ and $^3P_1$ to the ground $^1S_0$ state occur in the spectrum; the spontaneous emission rates[1,2] are respectively 7.7×10^8 s^{-1} and 8.33×10^6 s^{-1}; in absorption the $^1P_1$–$^1S_0$ line is 36-fold stronger than the $^3P_1$–$^1S_0$ line. The $^3P_0$ and $^3P_2$ states are both metastable. The electronic wave function of Hg($^3P_0$) changes sign when reflected in a plane through the nucleus; consequently collision complexes with an inert gas atom have the 0^- representation, and emission to the ground 0^+ states is therefore forbidden because of the $+ \not\leftrightarrow -$ rule. Thus collisionally induced emission from Hg($^3P_0$) by the inert gases is not observed. However, Hg($^3P_2$) can undergo induced emission due to collisions of inert gases.[3]

None of the states with the 6s6p configuration undergo significant collisional deactivation by the inert gases, with the exception of Xe.[3]

Traditionally, deactivation of Hg($^3P_1$) has been studied using CW excitation with 2537Å radiation from a resonance lamp; rate coefficients relative to the atomic emission rate are then derived by observing the attenuation of the intensity on addition of quenching gas.[4]

$$\mathrm{Hg}(^1S_0) + h\nu(2537\text{Å}) \rightarrow \mathrm{Hg}(^3P_1)$$

$$\mathrm{Hg}(^3P_1) \xrightarrow{k_f} \mathrm{Hg}(^1S_0) + h\nu$$

$$\mathrm{Hg}(^3P_1) + \mathrm{Q} \xrightarrow{k_q} \text{removal of Hg}(^3P_1)$$

Such a scheme leads to

$$I_0/I = 1 + k_q[\mathrm{Q}]/k_f$$

where I_0 is the intensity of the 2537Å fluorescence, and I that in the presence of added quenching gas Q. Thus plots of I_0/I vs. [Q] yield k_q, because k_f is known. Some values recommended in ref 5a are listed in Table I. More recent data may be found in ref 5b.

Measurement of quenching rates is complicated because of imprisonment of the resonance radiation; it is necessary to use very small pressures of Hg, and to extrapolate to zero [Hg]. It is further complicated because the imprisoned lifetime is a function of the pressure of added gas due to pressure broadening. Such changes in the effective lifetime of $^3P_1$ are illustrated by the results of Figure 2.

A direct measurement of the shortened lifetime of $^3P_1$ due to collisional removal has been reported, in which

0009-2665/87/0787-0335$06.50/0

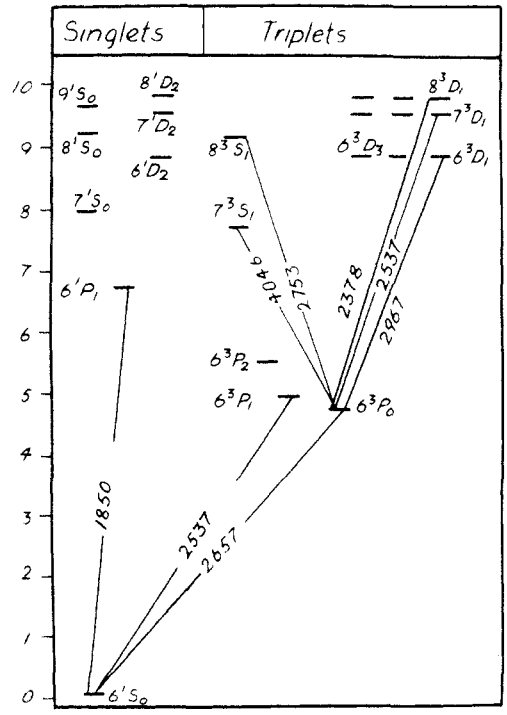

Figure 1. Energy levels of atomic mercury.

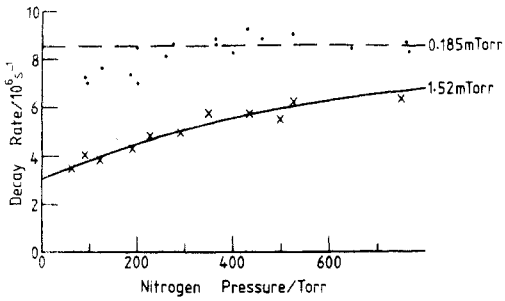

Figure 2. Variation of the effective emission rate of $Hg(6^3P_1)$ with nitrogen pressure. [Hg] = 0.18 mtorr •; [Hg] = 1.52 mtorr ×.

TABLE I. Rate Coefficients for Deactivation of $Hg(^3P_1)$ and $Hg(^3P_0)$, and Quantum Yields for $Hg(^3P_0)$ Formation (300 K)

	quenching coefficient, cm^3 $molecule^{-1}$ s^{-1}		$\Phi^3P_1 \rightarrow {}^3P_0$	
	$^3P_1$	$^3P_0$	ref 8	ref 9
N_2	4.3×10^{-12}		1.0	1.0
H_2	4.8×10^{-10}	5.37×10^{-11}		<0.03
O_2	3.0×10^{-10}	1.81×10^{-10}		<0.1
CO	9.3×10^{-11}	1.03×10^{-11}	0.88	0.9
NO	5.5×10^{-10}	2.5×10^{-10}		<0.1
NH_3	8.4×10^{-11}		1.05	0.64
C_2H_6	2.5×10^{-12}	8.9×10^{-14}	0.64	0.67
CO_2	4.6×10^{-11}	4.4×10^{-13}	<0.01	~0.02

the system was excited with very short pulses of radiation—10 ns—from a specially designed lamp.[7] Such a method, which gives the quenching rate directly, avoids uncertainties due to imprisonment.

Before proceeding to the more complex problems of molecule formation, we note that collisional relaxation of $^3P_1$ may occur directly to the ground $^1S_0$ state, or else populate the $^3P_0$ state; the energy difference between $^3P_1$ and $^3P_0$ is 1767 cm^{-1}. Quantum yields for metastable atom formation in the quenching of $^3P_1$ are given in Table 1. Those of ref 8 were derived by using CW excitation of gas mixtures, and monitoring the stationary $^3P_0$ concentrations by reversal of the 7^3S_1–6^3P_0 line generated with a second mercury lamp. The extent of spin–orbit relaxation depends on the competitive rate of reactions causing deactivation to $^1S_0$.

The data of ref 9 in Table I were obtained using a multielectrode, transverse discharge, resonance flash lamp, of the type shown in Figure 3. Through the outer jacket of the lamp are sealed 20 electrode pairs, supplied from a common distributor. The inner reaction vessel lies along the vessel axis and absorbs resonance radiation generated in the outer annulus. Much of our research on excited mercury intermediates has been conducted with these devices, which for absorption measurements are about 1 m in length, and about 30 cm for emission work; the lamps are usually repetitively pulsed with signal averaging. The same techniques have been applied to reactions photosensitized by Cd and Xe.[10]

The Hg,N_2 system is specially important and forms the basis for many applications. When excited with short duration pulses of 2537 Å radiation, an afterglow emission from $^3P_1$ is observed with a mean lifetime of ~250 μs with 700 torr of N_2 (300 K). There is negligible deactivation of $^3P_0$ to the $^1S_0$ mercury ground state by N_2.

$$Hg(^3P_1) + N_2 \underset{k''}{\overset{k'}{\rightleftharpoons}} Hg(^3P_0) + N_2$$

$$Hg(^3P_1) \xrightarrow{k_f} Hg(^1S_0) + h\nu$$

Because the $^3P_1$ is several orders of magnitude shorter lived than the delayed fluorescence, steady state can be assumed.

$$(k_f + k'[N_2])[^3P_1] = k'[^3P_0][N_2]$$

Therefore,

$$\frac{d[^3P_0]}{dt} = k'[N_2][^3P_0] - k'[N_2][^3P_1]$$

$$\tau^{-1} = -\frac{d \ln [^3P_0]}{dt} = \frac{k_f k'[N_2]}{k_f + k'[N_2]}$$

where τ is the mean lifetime of the luminescence. Using the value of k' listed in Table I, and obtaining k'' by calculating the $[^3P_0]/[^3P_1]$ equilibrium constant (1.87×10^3 at 297 K), $\tau = 2.4 \times 10^{-4}$ s is obtained with N_2 at 600 torr. The lifetime of the luminescence progressively increases as the pressure is reduced to ~50 torr, but at lower pressures decreases again due to wall loss of $^3P_0$. Extremely high levels of purity are required, and it is normal to continuously circulate the gases through a purifying system.

The Hg,N_2 system is richly rewarding when applied to determine the properties of $^3P_0$, i.e., relaxation, attachment, and dimer formation. Its special importance results from a negligibly small rate of deactivation of $^3P_0$ to $^1S_0$ in collision with N_2, so that a reservoir of metastable atoms is generated at relatively high concentration. Associated with the delayed 2537-Å fluorescence is a pressure broadened wing, due to N_2 collisions with the excited atoms, which can be monitored well into the visible region. This pressure broadened emission is due to the $Hg(^3P_1)$, N_2 collision complex; any emission from the $Hg(^3P_0)$, N_2 complex is too weak to detect. The electronic absorption spectrum of the $Hg(^1S_0)$, N_2 van der Waals molecule to the

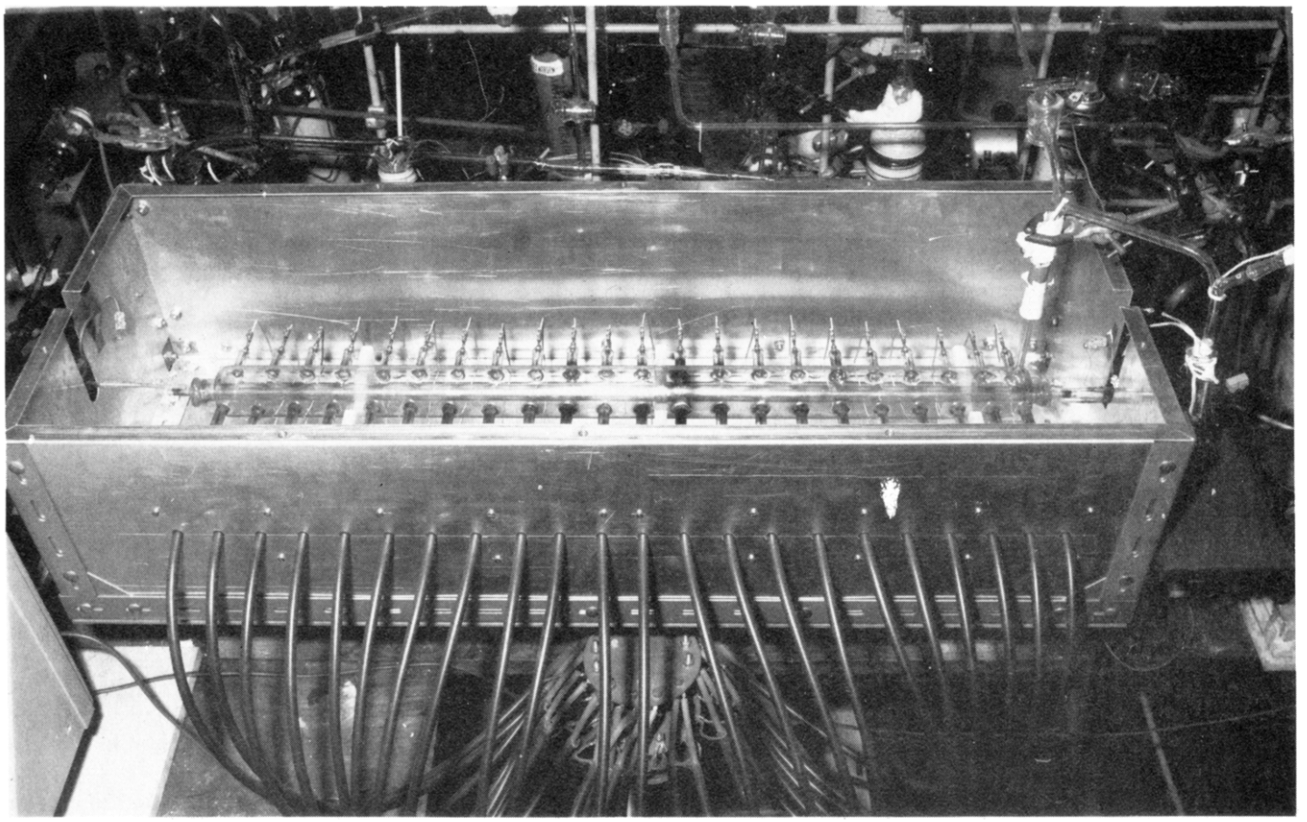

Figure 3. A multielectrode resonance flash lamp.

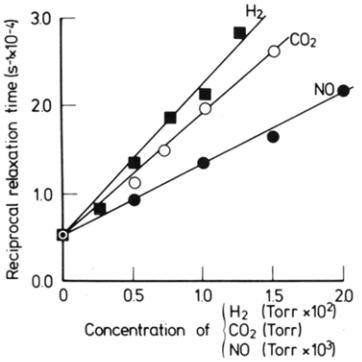

Figure 4. Dependence of the decay rate of $Hg(6^3P_0)$ on the partial pressure of added gas. Hg = 2×10^{-3} torr. 600 torr, N_2; ■, H_2; ○, CO_2; ●, NO.

$Hg(^3P_1)$, N_2 complex has been recorded in a supersonic free jet, and also its predissociation to $^3P_0$ plus N_2 has been demonstrated.[11a]

If a gas, Q, is added which will deactivate $^3P_0$ to the ground state with a rate coefficient k_q, the mean lifetime of the delayed fluorescence is reduced.

$$\tau^{-1} = \frac{k_f k'[N_2]}{k_f + k'[N_2]} + k_q[Q]$$

Examples of application are shown in Figure 4 for Q = H_2, CO_2, and NO. Some coefficients obtained from such experiments are included in Table I. Subsequently, two other groups have made similar measurements and the results are in broad agreement.[11b,12]

Efficient electronic quenching occurs when there are potential energy surfaces connecting the initial and final states in the classically accessible energy region; a strong attractive interaction of the excited atom and the quenching molecule causes the potential energy surface to converge with that of a lower electronic state. The interaction may be of two kinds, either donation of σ electrons from the quencher to the vacant 6s orbital of the excited atom, or donation of the 6p electron to the quenching molecule which then acts as a π acceptor. Molecules such as H_2S, PH_3, NO, and CO can simultaneously act in both capacities, and the bonding should be particularly strong.[9] A few structures for equilibrium conformations of intermediate collision complexes, derived from these considerations, are listed in Table II.

TABLE II. Proposed Structures for Intermediate Collision Complexes of $Hg(^3P)$

	bond type	structure	symmetry
H_2	π	H–H–Hg	C_{2v}
CO	$\sigma\pi$	HgCO	$C_{\infty v}$
H_2O	σ	H_2OHg	C_{2v}
NH_3	σ	H_3NHg	C_{3v}

Reaction of both $^3P_1$ and $^3P_0$ with H_2 produces substantial yields of HgH, Φ = 0.67 and 1.0, respectively. Curiously, in the reactions with HD the product is predominantly HgD. The attack of the $Hg(^3P)$ is presumably sideways on, to form the structure with C_{2v} symmetry of Table II; ejection of the light H atom from the complex is favored because of the smaller momentum requirement.[13]

Little is known concerning collisional relaxation of $Hg(^3P_2)$. The mercury laser[14] operates on the $7^3S_1 \rightarrow 6^3P_2$ line; N_2 at 10 torr is sufficient to depopulate the lower level[15a] and maintain population inversion, indicating that the coefficient for $^3P_2$ relaxation by N_2 is $\sim 10^{-10}$ cm^3 molecule^{-1} s^{-1}, much larger than for $^3P_1$. It may be significant that the reaction

$$Hg(^3P_2) + N_2(v = 0) \rightarrow Hg(^3P_1) + N_2(v = 2)$$

is closely resonant, $\Delta E = 2$ cm^{-1}. The $^3P_2$ does not undergo any significant relaxation to the lower spin–

orbit states in collision with $^1S_0$.[25] It is efficiently relaxed to $^3P_1$ by H_2O vapor.[3]

Relative cross sections for the $^3P_2 \rightarrow {}^3P_1$ relaxation by H_2, D_2, N_2, NO, and CH_4 have been measured with crossed molecular beam techniques.[15b]

Collisional relaxation of $Hg(^1P_1)$ has been pioneered using cw excitation, by studying both the attenuation of the intensity of the $^1P_1 \rightarrow {}^1S_0$ resonance line at 1849.5 Å on addition of quenching gases and also the associated emission at 2537 Å due to the collisionally induced $^1P_1 \rightarrow {}^3P_1$ transition.[16-18]

It has recently been discovered that, because the 1849Å line is 36-fold stronger than the 2537 Å line, by using very low Hg pressures in a resonance flash lamp and experimental cell, at least 90% of excitation can be achieved at 1849 Å.[3] Collisional population of $^3P_1$ from $^1P_1$ could then be time resolved. It is found that deactivation of $^1P_1$ by N_2 populates the $^3P_1$ level directly. Only 10% generates $N_2A^3\Sigma_u^+$, which can be identified by the rate at which it retransfers energy back to $Hg(^1S_0)$ to excite the ^3P states. The results indicate that the half pressure for quenching of $^1P_1$ by N_2 is ~40 Torr, corresponding to a coefficient of 5×10^{-10} cm^3 molecule^{-1} s^{-1}.

These experiments bring into perspective the possibility of laser action on the 2537-Å resonance line, by pumping at 1849 Å. The half pressure for the $^3P_1 \rightarrow {}^3P_0$ transition, induced by N_2, is 59 torr. Extremely small Hg pressures are required, with N_2 at ~40 torr. Because of the 3-fold degeneracy of the upper state, the $[^3P_1]/[^1S_0]$ ratio must exceed 3 for lasting action to be achieved.

II. Dimers and Trimers

The green emission of mercury vapor, the so called 4850-Å band, has been the subject of many kinetic and spectroscopic investigations, going back well over half a century. Recently there has been considerable progress in identifying the reactions which occur when Hg vapor absorbs radiation, and results in the formation of excited dimers. Model calculations[19,20] indicate that the first excited term of Hg_2 is $^3\Pi_g$; the $0_g^\pm$ components have very nearly the same energy and should comprise the first excited states of the dimer, as shown schematically in Figure 5. The electric dipole transition from these electronically excited states to the 0_g^+ ground state is forbidden, so that the $A0_g^\pm$ are expected to be optically metastable and hence long lived.

Studies of the decay of the luminescence, following pulsed laser excitation of pure Hg vapor at 2650 Å, have suggested that the carrier of the persistent green emission is an Hg_3* trimer, in equilibrium with excited dimers with high mercury densities.[21-23] The radiative

$$Hg_2^* + Hg \rightleftharpoons Hg_3^*$$

lifetime of the trimer has been estimated to be $\simeq 17$ μs.

From excited mercury vapor, emission is also observed in the ultraviolet—the 3350-Å band—and the upper state of the system has for a long time been identified with the $D1_u$ dimer, for which an electric dipole transition to the ground state is allowed. This assignment would now appear to be well established; vibrational relaxation of the $D1_u$ state has been investigated from the time variation of the fluorescence spectrum following direct optical excitation.[21]

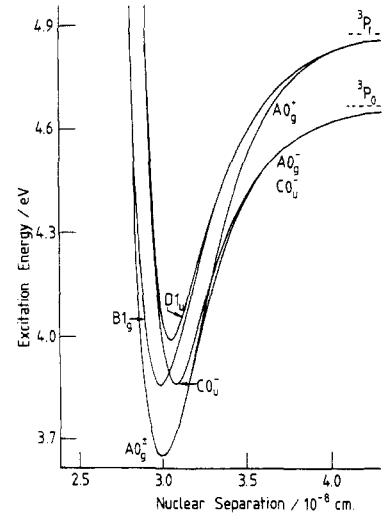

Figure 5. Schematic potential energy diagram for the first few excited states of the mercury dimer.

Our contribution has been directed at the spectroscopic detection of the transient intermediates by absorption spectroscopy, measurement of the rate coefficients for the termolecular formation of both dimers and trimers, identification of the reservoir states of the ultraviolet emission and the kinetics of their collisional relaxation, and finally determination of the fractions of atomic combination events leading to gerade and ungerade dimer states. The last problem may be understood by inspection of Figure 5; combination of $^3P_0$ with a ground state atom can occur adiabatically into either the $A0_g^-$ or $C0_u^-$ dimer state.

To record the spectra of the intermediates, the classical white-flash photolysis technique was employed: many entirely new features were discovered.[24,25] The initiating flash reached its maximum 5 μs after triggering, and had effectively terminated after a delay of 12 μs. The lamp and reaction vessel had a length of 1 m, and could be heated to 1000 K. The gases and Hg vapor were continuously purified by circulation.

Initially light is absorbed in continua which lie predominantly to the long wavelength of the 1849-Å and 2537-Å resonance lines. The continua are transitions from ground state van der Waals dimers to ungerade upper electronic states.

In Figure 6, absorption spectra are compared in an Hg,Ar mixture to those in an Hg,N_2 mixture. In both sets of spectra, several Rydberg transitions from excited mercury dimers may be seen, all of which exhibit extensive vibrational structure.

There are, however, several major differences between the results with Ar and N_2 added to the Hg vapor. In Ar, strong absorption is observed from each of the ^3P states, while in N_2 only transitions from $^3P_0$ are strong. The N_2, of course, induces transitions between the atomic states, and the relative populations are in equilibrium at the flash termination. The Ar results show that collision of $^3P_1$ and $^3P_2$ with ground state Hg atoms is remarkably ineffective at causing intramultiplet relaxation, even though the various diatomic states belonging to different limits merge and cross during collision. The decay rates of the excited atoms are represented diagramatically in Figure 7.

Some 15 band systems of excited mercury dimers were identified and analyzed; only one of these had

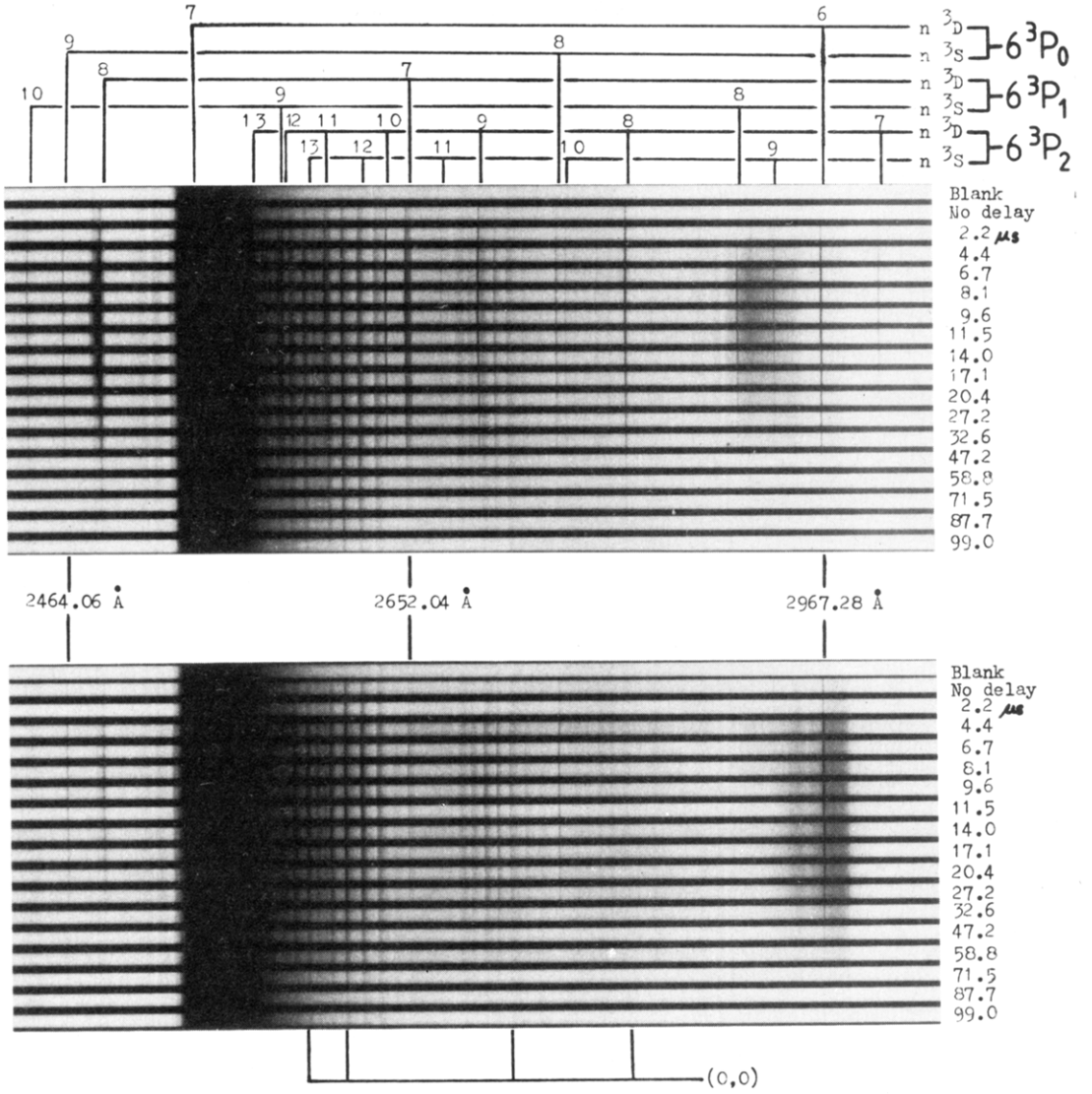

Figure 6. Comparison of transient spectra in mixtures of Hg vapor with Ar (upper set) and N_2 (lower set). Delay times on the right. [Hg] = 110 torr; [Ar] = [N_2] = 200 torr (550 K).

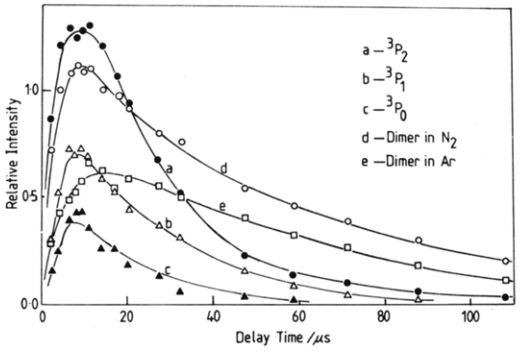

Figure 7. Time variation of transient spectra (560 K): a,b,c, and e; [Hg] = 110 Torr; [Ar] = 200 torr; d[Hg] = 110 torr; [N_2] = 200 torr.

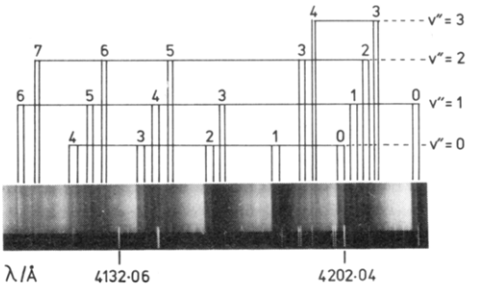

Figure 8. Absorption spectrum of the 4200-Å system of the mercury dimer, and a partial vibrational analysis.

previously been observed in emission and analyzed.[26] Nearly all the strong systems are due to transitions of Hg_2 $A0_g^{\pm}$, which constitutes the reservoir to fuel the persistent green emission. It was considered a significant advance to see these reservoir states, the existence of which had long been suspected in some form, but never before observed directly.

An enlargement of the 4200-Å system is shown in Figure 8. The bands are doubled, with a splitting of 15.5 cm^{-1} in the $v'' = 0$ progression. The same feature is found in three of the other dimer systems, and apparently corresponds to the energy difference between the 0_g^+ and 0_g^- components. The two members of each band pair uniformly have about the same intensity or Franck–Condon factor. The splitting decreases with increasing v'', and the two potential energy curves must cross at an energy of $\simeq 10^3$ cm^{-1}; therefore the 0_g^+ component has to be the first excited state of the mercury dimer. The vibrational frequency is 143 cm^{-1}. The upper Rydberg states all have vibrational frequencies of $\simeq 120$ cm^{-1}, which must correspond closely to that

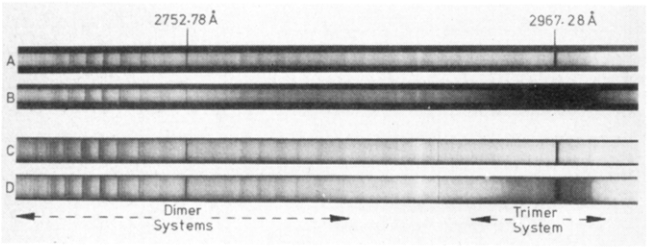

Figure 9. Effect of [Hg] and temperature on the mercury trimer band intensity. (A) [Hg] = 24 torr, flash energy 500 J (560 K); (B) [Hg] = 75 torr, flash energy 280 J (560 K); (C) [Hg] = 230 torr, flash energy 1620 J (773 K); (D) [Hg] = 90 torr, flash energy 1620 J (550 K).

of the ground electronic state of the Hg_2^+ positive ion.

Some of the weaker band systems increase in intensity relative to those from $A0_g^{\pm}$ with increasing temperature. A system at 4514 Å has been tentatively assigned to the $B1_g$ carrier; by measuring the variation of relative intensity with temperature, the difference of electronic energy between the $A0_g^{\pm}$ and $B1_g$ states has been estimated to be $\simeq$1700 cm^{-1}. Other electronic systems have been tentatively assigned to the $C0_u^-$ carrier. With the high mercury pressures that are required for the white flash experiments, the excited dimer states are in mutual equilibrium.

Considering again the time-resolved spectra of Figure 6, next to be discussed is the nature of the very strong continuous absorption, in the region of the 2967-Å atomic line, which is observed in N_2, Hg mixtures. It has been shown that the ratio of the concentration of the carrier of these diffuse bands to the concentration of dimers is proportional to [Hg], and independent of the delay time.[25] Conditions were adjusted so that approximately the same dimer concentrations were attained, varying both flash energy and [Hg]. Also, the diffuse spectra are weakened relative to the dimer bands by increase of temperature due to changes of the equilibrium constant. These effects of both concentration and temperature are illustrated in Figure 9. The continuous band can be unequivocally assigned to an excited mercury trimer; from the kinetic data presented later, evidently it is the carrier of the green emission. The trimer exhibits other regions of diffuse absorption, and the full spectrum is shown in Figure 10.

The first excited terms of linear Hg_3 are $^3\Pi_u$ and $^3\Sigma_u^+$. Of these, the 0_u^+ state and the two 1_u states can decay by emission to the ground state. There are no model calculations for the trimer. The 0_u^+ component is expected to be the carrier of the green band.

The dimers and trimers coexist close to equilibrium with high [Hg] and with added N_2. From a quantitative study of the relative dimer and trimer band intensities over a range of temperatures, the energy required to dissociate an atom from the trimer has been shown to be 0.57 (±.03) eV.[25]

$$Hg_2\ A0_g^{\pm} + Hg(^1S_0) \rightleftharpoons Hg_3\ A0_u^{\pm}$$

$$Hg_3\ A0_u^{+} \rightarrow 3Hg(^1S_0) + h\nu\ \text{(green band)}$$

Considering again the absorption spectra of Figure 6, it is most remarkable that with added Ar the trimer band at 3000 Å is quite weak, but a diffuse feature not observed in N_2 occurs at a shorter wavelength! With higher [Hg], the trimer bands observed in N_2, Hg mixtures do appear slowly in the Ar, Hg system, possibly indicating that the shorter wavelength carrier is slowly converted to the first excited states of the trimer by collision with $Hg(^1S_0)$. We do not have sufficient kinetic data concerning this diffuse band to be able to make an assignment.

The final aspect of the spectra of Figure 6 to be briefly considered is the appearance of the 2480-Å group

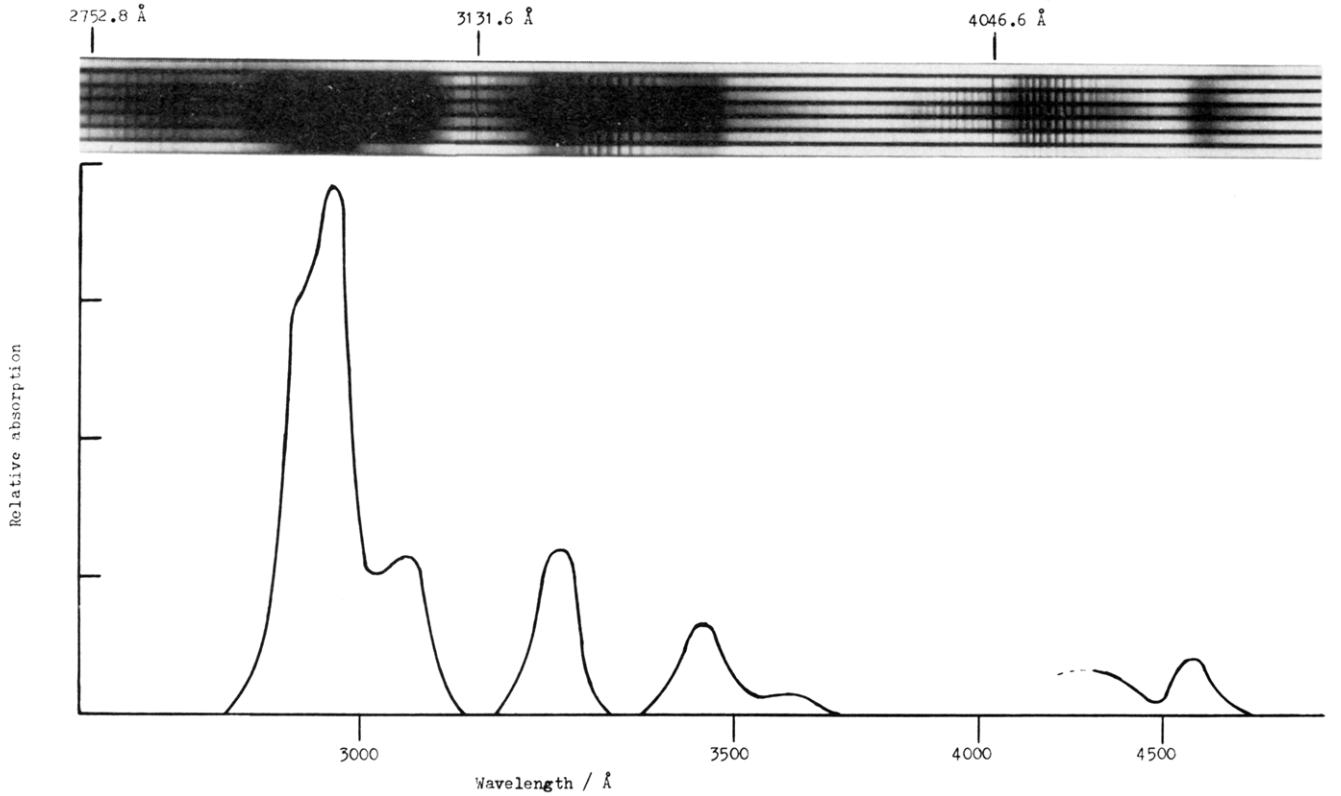

Figure 10. Electronic spectra of the mercury trimer. Delay time increasing from top to bottom. [Hg] = 120 torr (550 K).

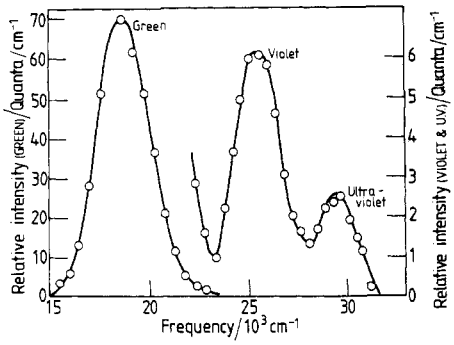

Figure 11. Emission spectrum in the afterglow following pulsed excitation at 2537 Å. Left hand scale green only. $[N_2]$ = 760 torr, [Hg] = 0.18 mtorr (298 K).

of bands, which is strong with Ar, Hg mixtures but usually comparatively weak with added N_2. These bands are well-known in emission from discharges, but had not previously been detected in absorption. In the old literature,[27] the system is assigned to a transition of the Hg_2^+ positive ion. At first, it was difficult to accept that a molecular ion could be generated at sufficiently high concentration in a flash photolysis experiment to give rise to such a strong absorption. However, after a long and not very conclusive study it is considered that Hg_2^+ probably is the carrier; the species can be produced by Hornbeck–Molnar ionization of high-energy states of the neutral atom in collision with a ground-state atom.

$$Hg^* + Hg(^1S_0) \rightarrow Hg_2^+ + e^-$$

These comments complete a description of the results from the white-flash photolysis of Hg vapor. The formation of a reservoir of metastable dimers, in equilibrium with trimers in an excess of added N_2, is revealed by these experiments. Some of the other discoveries have not been fully analyzed, and will require application of other techniques.

To measure the rate coefficients for the elementary steps, the resonance flash method has been employed, with a transverse discharge multielectrode lamp surrounding a coaxial reaction vessel. To achieve the required Hg pressures, the gases were first passed through a heater containing liquid mercury, and then through a glass spiral contained in a thermostat to condense out the excess. By replacing the thermostat with a cold trap, the mercury vapor could be removed in a few minutes and the level of background emission recorded. The gases were continuously circulated and repurified. The exciting flash of 2537-Å resonance radiation decayed to one half of the maximum intensity after 1.5 μs, and was of neglibly short duration compared with that of the excited intermediates.

We first consider a comparatively simple experiment in which a high pressure of N_2 is maintained; N_2 rapidly interconverts the gerade and ungerade dimer states which therefore attain mutual equilibrium.

The luminescence is very persistent, and the signal to noise ratio is high even after 10-ms delay. A spectrum recorded after a fixed time delay in the late afterglow is shown in Figure 11. In addition to the well-known green band (trimer) and UV band (1_u dimer), an intermediate violet band was discovered.[28] By measuring the intensities of the new feature relative to the green and UV bands, it has been concluded that it

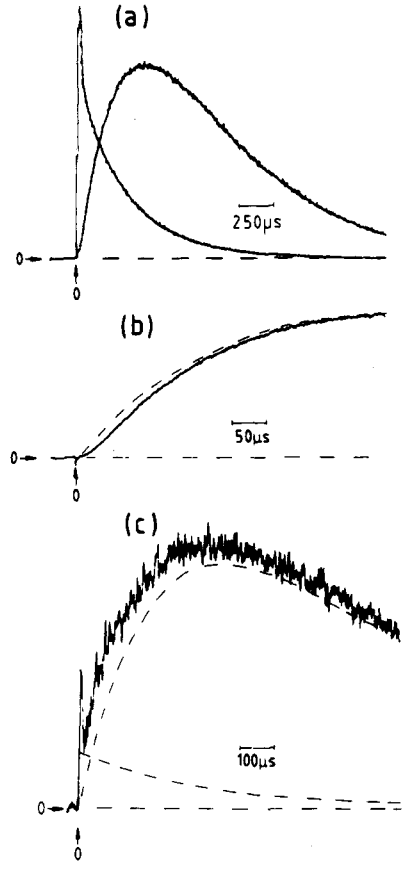

Figure 12. Time evolution of luminescence following pulsed excitation at 2537 Å. (a) Descending short-lived trace delayed 2537 Å emission; initially rising trace green emission. (b) Full trace rise green intensity. Dashed curve calculated $[Hg_2\ 0_g^{\pm}]$. (c) Full trace violet emission. Dashed curves wing of 2537 Å line, and the residue found by subtraction.

results from collisionally induced emission from the $A0_g^{\pm}$ dimer to the ground state. At short delay times both the UV and violet bands are swamped by the pressure-broadened 2537-Å delayed fluorescence.

Some time profiles of the green and violet components at 304 K are shown in Figure 12. It is convenient to state the reaction mechanism at this stage.

$$Hg(^1S_0) + h\nu\ (2537\ Å) \rightarrow Hg(^3P_1)$$

$$Hg(^3P_1) + N_2 \rightleftarrows Hg(^3P_0) + N_2$$

$$Hg(^3P_0) + Hg(^1S_0) + M \xrightarrow{k_1} Hg_2\ A0_g^{\pm} + M$$

$$Hg_2\ D1_u \xrightarrow{k_2} 2Hg(^1S_0) + h\nu\ (UV)$$

$$Hg_2\ A0_g^{\pm} + N_2 \xrightarrow{k_3} 2Hg(^1S_0) + N_2 + h\nu\ (violet)$$

$$Hg_2\ A0_g^{\pm} \xrightarrow{k_4} \text{zero pressure loss rate}$$

$$Hg_2\ A0_g^{\pm} + Hg(^1S_0) + M \underset{k_{-5}}{\overset{k_5}{\rightleftharpoons}} Hg_3\ A0_u^{\pm} + M$$

$$Hg_3\ A0_u^{\pm} \xrightarrow{k_6} 3Hg(^1S_0) + h\nu\ (green)$$

Reaction 1 produces both gerade and ungerade dimer states; however, since N_2 rapidly maintains equilibrium between these states,[6] the details need not concern us at this stage of the discussion.

Considering Figure 12a, the descending trace is the delayed 2537-Å fluorescence resulting from excitation

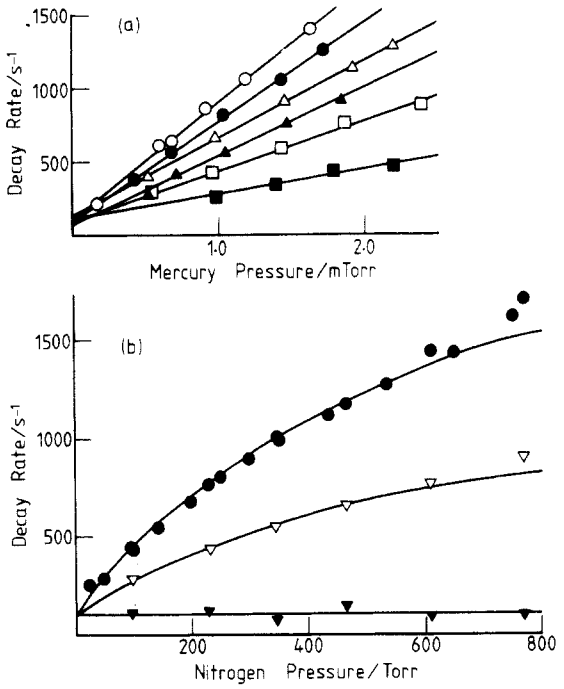

Figure 13. First-order decay coefficients of the green emission in the late afterglow (304 K). (a) N_2 in torr: 750 ○; 610 ●; 465 △; 345 ▲; 230 □; 97 ■. (b) Hg in mtorr: 1.0 ●; 1.0 ▽; 0.0 ▼.

of $^3P_0$ to $^3P_1$ by N_2 collisions. The initially rising trace is the time profile of the green emission; because the radiative lifetime of the trimer is short compared with the duration of the afterglow, the profile of the green emission is a measure of the relative concentration of the $Hg_2\ A0_g^{\pm}$ reservoir states, produced by reaction 5. With these conditions only $\simeq$2% of the $^3P_0$ combine to form dimers, the great excess decaying by the delayed 2537-Å fluorescence.

The initiating pulse of resonance radiation is of negligibly short duration in these experiments. Because both the formation and the loss of $Hg_2\ A0_g^{\pm}$ are pseudo-first-order, the full time profile should approximate to a double exponential function:

$$[\exp(-\alpha t) - \exp(-\beta t)]/(\beta - \alpha)$$

Here β corresponds to the $^3P_0$ decay rate and α to the metastable dimer decay rate. In Figure 12b, however, it may be noted that there is an inflection on the rise of the green band due to the finite radiative lifetime of the trimer, which is computed to be $\simeq 2 \times 10^{-5}$ s, derived from the experiments using laser excitation of Hg vapor at high densities.[23]

Figure 12c shows the time profile in the violet region. The emission is again a double exponential, but in this case with unequal coefficients because the emission in this region is a superposition of the violet band shown in Figure 11 and the N_2 pressure broadened wing of the 2537-Å line. The residue found by subtraction of the resonance wing has a time profile indistinguishable from that of the green emission. In the intermediate and late afterglow, the relative intensities of the three bands are time independent, the green being predominant.

These comments complete a description of the nature of the delayed emissions, and their dependence on time. In the late afterglow when the $^3P_0$ concentration is small, the decay of the emission is indistinguishable from a single exponential term.[6] The corresponding rates have been measured in N_2, Hg mixtures at 304 K, 333 K, and 363 K. Some results for 304 K are shown in Figure 13. In (a) it may be noted that the decay of the dimer reservoir states is proportional to [Hg] for all $[N_2]$, and increases with $[N_2]$; these rates correspond to termolecular attachment of $Hg(^1S_0)$ to $Hg_2\ A0_g^{\pm}$ with N_2 as third body, forming excited trimers by reaction 5. In 13b, the same data are displayed as a function of $[N_2]$, and nonlinear behavior is found; the latter feature is due to reverse dissociation of trimer back to the $Hg_2\ A0_g^{\pm}$ reservoir state.

Also in 13b is included a set of points for [Hg] extrapolated to zero; there appears to be a zero mercury decay component of the reservoir states amounting to $\simeq 85 s^{-1}$, which is apparent at all temperatures. This minor component may be due, at least in part, to internal conversion of $Hg_2\ A0_g^+$ to the dimer ground state. Some rate coefficients derived from these data are listed in Table III.

It is the combination of the spectroscopic data of Figures 6, 9, and 10, revealing the existence of an excited trimer in this system, with the kinetic data which shows that the $Hg_2\ A0_g^{\pm}$ decays by termolecular attachment of a third Hg atom, that establishes that the green carrier is a bound, excited trimer. The intensity of the green band relative to the UV emission does, of course, increase with increasing [Hg].

TABLE III. Rate Coefficients for the Mercury Dimer and Trimer Systems[29-31]

M	k_1, 10^{-31} cm^6 molecule^{-2} s^{-1} 303 K	353 K
	$Hg(^3P_0) + Hg(^1S_0) + M \xrightarrow{k_1} Hg_2^* + M$	
Ar	0.97 (±0.08)	0.95 (±0.06)
Ne	0.39 (±0.06)	0.33 (±0.06)
He	0.31 (±0.07)	0.22 (±0.06)
N_2	1.56 (±0.15)	1.22 (±0.12)
	$k_1^u/k_1^g = 0.124$ (±0.014) (303 K)	

$Hg_2\ D1_u \xrightarrow{k_2} 2Hg(^1S_0) + h\nu$ (ultraviolet)[a]
$k_2 = 1.5 \times 10^6$ s^{-1} with $\Delta E(1_u - 0_g^{\pm}) = 0.33$ eV (303 K)
$k_2 Q_{D1_u}/Q_{C0_u^-} = 1.23$ (±0.03) $\times 10^4$ s^{-1} (303 K)
$k_2 Q_{D1_u}/Q_{C0_u^-} = 2.15$ (±0.02) $\times 10^4$ s^{-1} (343 K)

$Hg_2\ A0_g^{\pm} + N_2 \xrightarrow{k_3} 2Hg(^1S_0) + N_2 + h\nu$ (violet)[a]
$k_3 = 2.9$ (±0.03) $\times 10^{-19}$ cm^3 molecule^{-1} s^{-1} (298 and 333 K)

$Hg_2\ A0_g^{\pm} \xrightarrow{k_4}$ Zero Pressure Loss Rate
$k_4 \simeq 85$ s^{-1}

$Hg_2\ A0_g^{\pm} + Hg(^1S_0) + M \xrightarrow{k_5} Hg_3^* + M$
$k_5(M = N_2) = 1.95$ (±0.16) $\times 10^{-30}$ cm^6 molecule^{-2} s^{-1} (304 K)
$k_5(M = N_2) = 1.49$ (±0.03) $\times 10^{-30}$ cm^6 molecule^{-2} s^{-1} (333 K)
$k_5(M = N_2) = 1.26$ (±0.05) $\times 10^{-30}$ cm^6 molecule^{-2} s^{-1} (363 K)
$k_5(M = Ar) = 1.36$ (±0.1) $\times 10^{-30}$ cm^6 molecule^{-2} s^{-1} (304 K)

$Hg_3^* + M \xrightarrow{k_{-5}} Hg_2\ A0_g^{\pm} + Hg(^1S_0) + M$
$k_{-5}/k_6\ (M = N_2) = 4.7$ (±0.1) $\times 10^{-20}$ cm^3 molecule^{-1} (304 K)
$k_{-5}/k_6\ (M = N_2) = 4.8$ (±0.15) $\times 10^{-20}$ cm^3 molecule^{-1} (333 K)
$k_{-5}/k_6\ (M = Ar) = 3.3$ (±0.3) $\times 10^{-20}$ cm^3 molecule^{-1} (304 K)

$Hg_3\ A0_u^+ \xrightarrow{k_6} 3Hg(^1S_0) + h\nu$ (green)[a]
$k_6 \simeq 5 \times 10^4$ s^{-1} (303 K)

$Hg_2\ C0_u^- + M \underset{k_{-7}}{\overset{k_7}{\rightleftharpoons}} Hg_2\ A0_g^{\pm} + M$
k_7 in units of cm^3 molecule^{-1} s^{-1}. All data 303 K.
$k_7^{Hg} = 1.66$ (±.1) $\times 10^{-10}$; $k_7^{N_2} = 2.95$ (±.2) $\times 10^{-14}$;
$k_7^{Ar} \leq 10^{-16}$; $k_7^{Ne} \leq 10^{-16}$; $k_7^{He} = 6.7$ (±1.0) $\times 10^{-16}$
$k_7/k_{-7} = 4.9 \times 10^3$

[a] Approximate short wavelength thresholds: green, 2.9 eV; violet, 3.6 eV; ultraviolet, 4.0 eV.

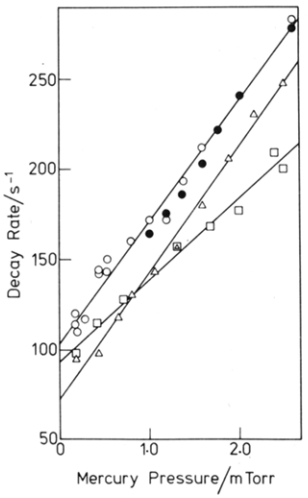

Figure 14. Variation of the $Hg(^3P_0)$ decay rate with pressure of Hg vapor (303 K). ○, ●, 710 torr Ar, 0.71 torr N_2 (hollow 3400Å, filled 5240Å); △, 750 torr Ar, 0.35 torr N_2; □, 400 torr Ar, 0.71 torr N_2.

Attention was next directed at the measurement of rate coefficients for dimer formation from $^3P_0$. In N_2 with pressures sufficiently high to prevent wall loss of $^3P_0$, the dominant mode of decay is via reexcitation to $^3P_1$ and delayed 2537-Å fluorescence; only a very small fraction of $^3P_0$ combines with $^1S_0$, so that this step does not significantly affect the kinetics. However, if the N_2 is kept very small, ~1.0 Torr, to limit the rate of reexcitation to $^3P_1$, and with comparatively high pressures of added Ar to chaperon dimer formation and avoid $^3P_0$ wall loss, the dimerisation rates can be measured directly.[29]

Results for $^3P_0$ decay with these conditions are shown in Figure 14, obtained, of course, by using the resonance flash technique. The zero mercury pressure intercepts correspond to reexcitation and emission of $^3P_1$. The most accurate measure of the relative $^3P_0$ concentration was achieved by monitoring the decay of the UV emission from Hg_2 $D1_u$, discussed later. The measurements yield the total coefficient for combination of $^3P_0$ with a ground-state Hg atom into both gerade and ungerade dimer states; data for Ar, Ne, and He as third bodies are included in Table III. There are no other systematic measurements of these coefficients.

With regard to the formation of excited dimers in mercury vapour, the most important rate coefficient is that with N_2 as third body. This coefficient was measured relative to that for Ar using a cw technique. In essence, the ratio is found by first observing the intensity of the green band in an Hg, N_2 mixture, and then studying the enhancement caused by addition of Ar. In practice it is complicated because of a drop in the $[^3P_0]$ on addition of Ar, and because of the zero pressure loss rate of Hg_2 $A0_g^{\pm}$. An accurate analysis was eventually developed and the derived coefficients are listed in Table III.

These measurements brought us to within striking distance of the heart of the mechanism of the persistent mercury luminescence, which is the relative roles of the gerade and ungerade dimers states, as shown in Figure 5. We have demonstrated previously that in high pressures of N_2 the relative intensities of the various emission bands are time invariant; the N_2 collisionally interrelaxes various dimer states which rapidly attain

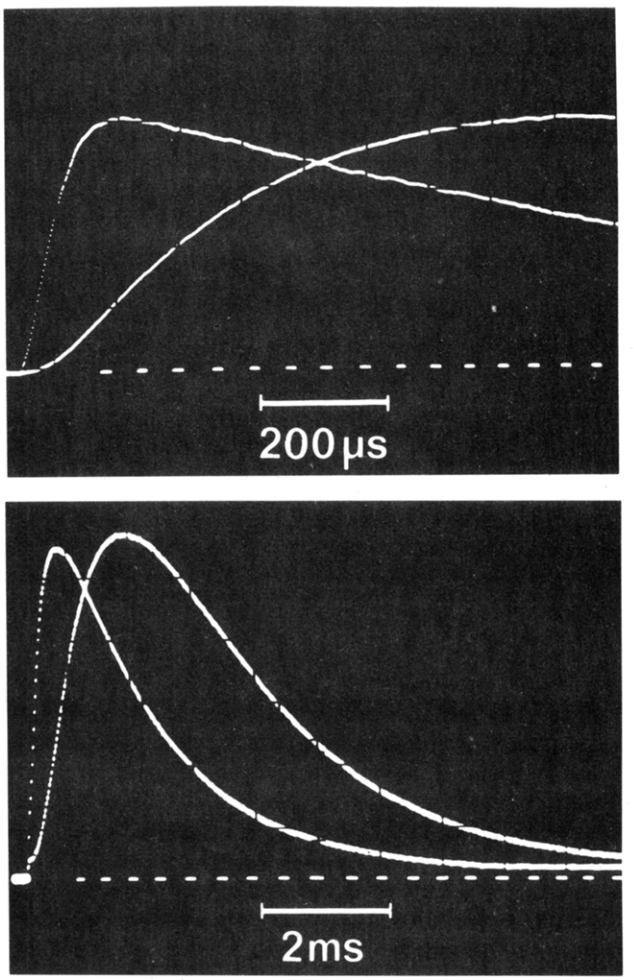

Figure 15. Time variation of ultraviolet and green emission following pulsed excitation at 2537 Å. The fast rising traces correspond to the UV component, which decays with the metastable atoms. The rise of the green intensity reflects the accumulation in the Hg_2 $A0_g^{\pm}$ reservoir (304 K). [Hg] = 2.4 mtorr, $[N_2]$ = 10 torr, [Ar] = 600 torr.

relative equilibrium populations. However, in experiments with small pressures of N_2, with an excess of Ar to produce dimers, the green and UV time profiles are quite different;[30] evidently Ar collisions do not efficiently interconvert the $D1_u$ and $A0_g^{\pm}$ dimer states.

Differences in the green and UV time profiles[31] are shown in Figure 15, with $[N_2]$ at 10 torr and [Ar] at 600 torr. The slowly rising trace is the green emission, the rise corresponding to the decay of $^3P_0$, and the decay to the rate of trimer formation from Hg_2 $A0_g^{\pm}$. The shorter lived trace corresponds to the UV emission. Ultraviolet reservoir states are formed and removed by pseudo-first-order processes in these experiments. The corresponding integrated rate equation is again a double exponential function,

$$(\exp(-\alpha t) - \exp(-\beta t))/(\beta - \alpha)$$

where the coefficients correspond to formation and loss rates. However, because the UV reservoir states are short lived compared to $^3P_0$, it is the removal rate of $^3P_0$ which shapes the decay of the UV band! This is subject to a minor qualification concerning the initial rise of the green band which exhibits an inflexion due to the finite lifetime of the trimer, and also because of delayed release of excited dimers from higher states into the $A0_g^{\pm}$ reservoir.

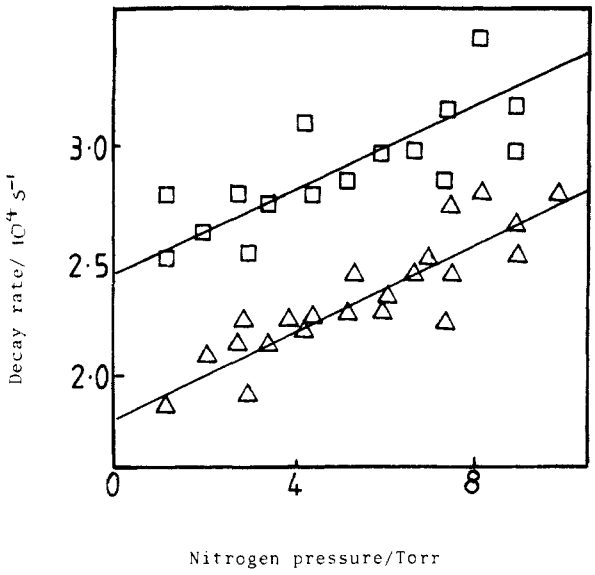

Figure 16. Variation of the decay rate of the ultraviolet reservoir on $[N_2]$ (303 K). □, [Hg] = 2.4 mtorr; △, [Hg] = 1.2 mtorr.

Because the rate of $^3P_0$ decay can be measured accurately, the decay rates of the ultraviolet reservoir can be extracted from the UV profile either by computer fitting or simply solving for the intensity maximum. Various sets of data were therby derived, for example, the results shown in Figure 16.

The emission rate of the $D1_u$ dimer[23] is believed to be $\sim 10^6$ s^{-1}; evidently, therefore, the observed time constant of a $\simeq 10^{-4}$ s for the species generating the UV emission indicates that there is a metastable reservoir from which the emitting state is populated by collisional processes. The results, for example, those of Figure 16, are not significantly affected if the pressure of Ar is varied in the range 300 to 700 torr. It must follow that with these high pressures of Ar the $D1_u$ dimer is in equilibrium with its reservoir states, and that Ar does not significantly deactivate the UV reservoir. Extrapolated to zero [Hg] and $[N_2]$, the effective decay rate of the UV reservoir is 1.23 (±.03) × 10^4 s^{-1} at 303 K. This is equivalent to k_2Q_{1u}/Q_{reser}, where k_2 is the emission rate of the $D1_u$ dimer, and the Q are partition functions.

In the experiments with excess N_2 described in an earlier subsection,

$$k_2Q_{1u}/Q_{0g}^{\pm} = 2.3\ (\pm.25)\ s^{-1}$$

was derived at 303 K. This measurement is made by comparing the extent of emission from $D1_u$ dimers with the known rate of formation of trimers from $Hg_2\ A0_g^{\pm}$. Thus,

$$Q_{reser}/Q_{0g}^{\pm} = 2(\pm.27) \times 10^{-4} \quad \text{(at 303 K)}$$

The relative energies of the dimer states given in Figure 5 are expected to be reliable to within 0.03 eV. The corresponding ratio of the partition functions for $C0_u^-$ to $A0_g^{\pm}$ is

$$Q_{0u}^-/Q_{0g}^{\pm} \simeq 2 \times 10^{-4}$$

at 303 K, being a good match with that measured experimentally for the ratio of the partition function of the reservoir state to that of $Hg_2\ A0_g^{\pm}$. Although the point is obviously not proven, the lifetime of the UV emission is consistent with $C0_u^-$ being the sole reservoir state.

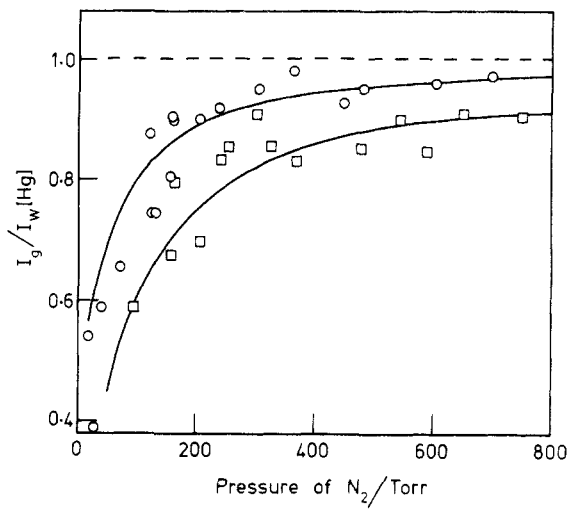

Figure 17. Variation of the quantum yield of the green emission relative to the total rate of dimer formation (ref 29). The full lines are calculated using the coefficients of Table III. ○, [Hg] = 2.0 mtorr; □, [Hg] = 0.76 mtorr.

With this hypothesis, the mechanism is tentatively completed as follows.

$$Hg(^3P_0) + Hg(^1S_0) + M \xrightarrow{k_1^u} Hg_2\ C0_u^- + M$$
$$Hg(^3P_0) + Hg(^1S_0) + M \xrightarrow{k_1^g} Hg_2\ A0_g^{\pm} + M$$

$$Hg_2\ C0_u^- + Ar \rightleftharpoons Hg_2\ D1_u + Ar$$

$$M + Hg_2\ C0_u^- \xrightarrow{k_7} Hg_2\ A0_g^{\pm} + M$$

Some measured k_7 are listed in Table III. Evidently collision with $Hg(^1S_0)$ very efficiently interconverts the dimer states, the reactions proceding through an intermediate excited trimer. (This is in curious contrast to the ^3P atomic states which do not interconvert in collision with $^1S_0$.)

The most recent episode in understanding the behavior of excited Hg vapor has been to measure the quantum yield of the 3350-Å UV emission relative to the formation of excited dimers by reaction 1.

If the quantum yield, Φ_g, of the green band, in various pressures of N_2, is examined as a function of partial pressures, it is found that, relative to the rate of formation of excited dimers, Φ_g tends to a limiting maximum at high pressures;[29] this maximum corresponds to unit quantum yield, and there is negligible deactivation of either $A0_g^{\pm}$ dimers or trimers by N_2. The effects of pressure arise because of nonradiative decay of $A0_g^{\pm}$ dimers by reaction 4; with $[N_2] \geq 100$ torr, the fraction, F, which decays the green emission is given by

$$F^{-1} = 1 + k_4/k_5[Hg][M] + k_4k_{-5}/k_6k_5[Hg]$$

This expression is compared to experiment in Figure 17, where the experimental method was to use cw excitation of N_2, Hg mixtures.

The relative UV and green intensities , I_{UV} and I_g, were integrated over the spectral profiles for various gas compositions, again using a cw technique. The spectral sensitivity of the detector was calibrated with light from

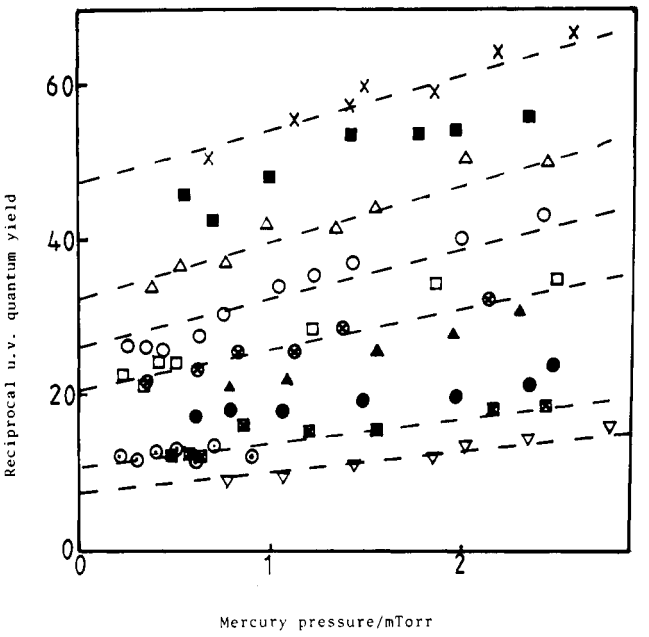

Figure 18. Quantum yields of the UV band, relative to the total rate of production of excited dimers (303 K). [Ar] ~660 torr unless indicated. [N_2] in torr as follows: ▽, 0.56; ▣, 0.52; ⊙, 6.0; ⊗, 21; □, 24.5; ○, 34.5; △, 44; ■, 54; ×, 61; ●, 9.7 (344 Ar); ▲, 17 (327 Ar).

a tungsten ribbon lamp. Quantum yields of the UV emission were then computed using,

$$\Phi_{UV} = I_{UV}/(I_{UV} + I_g F^{-1})$$

Some data so derived are shown in Figure 18. It may be noted that Φ_{UV} decreases with increasing [Hg] and [N_2], because both Hg and N_2 deactivate $C0_u^-$ dimers to the $A0_g^{\pm}$ reservoir of the green band.

The quantum yields for formation of the $C0_u^-$ dimer, relative to the total rate of formation of dimers by reaction 1, have been evaluated for each of the experimental points of Figure 18, by calculating from the rate cofficients of Table III the fraction of $C0_u^-$ dimers which result in UV emission under each set of conditions. The results of this analysis are shown in Figure 19. Thus

$$\Phi_{UV}^0 = k_1^u/(k_u^u + k_1^g) = 0.124\ (\pm 0.014)$$

is found.

The quantum yield of the UV emission is small even when extrapolated to zero pressure; approximately one combination occurs into a vibrationally relaxed $C0_u^-$ state per six or seven into the relaxed $A0_g^{\pm}$ reservoir.

To interpret this aspect, we first consider the consequences that the potential energy curves of the $C0_u^-$ and $A0_g^-$ dimer states are nearly coincident at long and intermediate range as shown in Figure 5. A $^3P_0$ atom can combine with a ground state atom adiabatically into either state. Because the Hg atoms have a much greater mass then those of the chaperon, only a small fraction of the total binding energy is removed, so that the initial phase of reaction 1 is to produce vibrationally excited dimers, with equal probability into each of the states. Because of the near coincidence of the large r turning points at intermediate range, the gerade and ungerade states will be mixed by subsequent relaxing collisions which perturb the electronic center of symmetry. At intermediate range, where the potential energy curves are beginning to diverge, the exothermic relaxation from the $C0_u^-$ to the lower $A0_g^-$ state starts to become "irreversible" when the energy difference is of the order of kT; the excitation then drains down disproportionately into the relaxed $A0_g^-$ reservoir. Further divergence at lower energies ultimately closes the route because the associated large changes of the reduced momentum have a low probability. Considering vibrationally relaxed dimers, only one in four originally born with the $C0_u^-$ representation survives the succession of subsequent collisions which remove the excess vibrational energy.

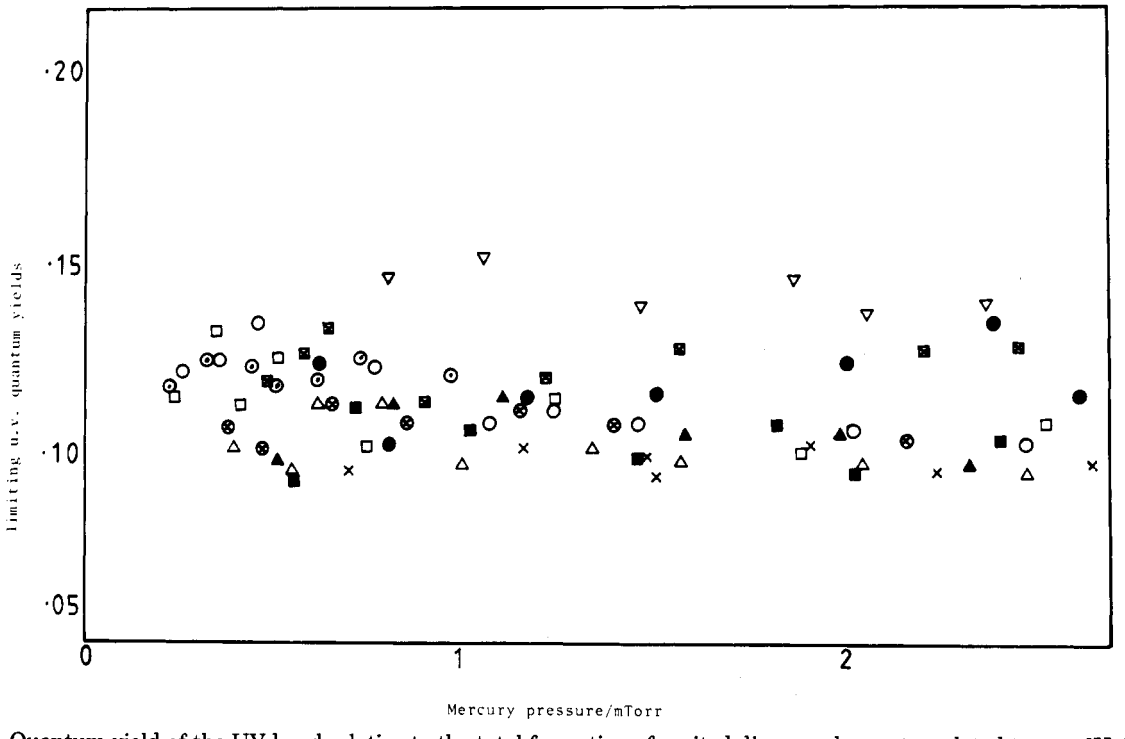

Figure 19. Quantum yield of the UV band relative to the total formation of excited dimers, when extrapolated to zero [Hg] and [N_2] (303 K).

The rate coefficients for the termolecular combination of $^3P_0$ with ground state Hg atoms are larger than those for two ground-state halogen atoms by a factor of about 10. Presumably the high rates are found because Hg($^3P_0$), Hg($^1S_0$) correlates with just two states, both of which are bound and participate in the combination reactions: formation of ground state halogen molecules has to compete with 15 other substates which correlate with repulsive or only weakly bound states.

These comments complete a description of the status quo in respect of mercury dimers and trimers.

The model calculations for the dimer states[19-20] have been of great value in both rationalizing the results and also as a predictive guide. Even so, more precise information concerning the excited states is sorely needed to test the arguments applied to identify the ultraviolet reservoir, and also to aid the assignment of dimer "hot" bands.[32a]

Calculations of the energies of the dimer states, using configurational interaction procedures for the valence electrons and ab initio effective potentials for the core, indicate that the $C0_u^-$ state may not be bound.[32b] If these calculations prove to be realistic, the ultraviolet reservoir state would have to be redefined to be the $B1_g$ excited dimer.

Our conclusions are broadly in agreement with high temperature and high Hg density experiments described in ref 21–23, in so far as close comparison can be made; considering both contributions together, identification of the green carrier with an excited mercury trimer is now quite compelling and soundly established.

Theoretical guidance on the states of the mercury trimer would also be of great value; the diffuse absorption band observed in flashed Hg,Ar mixtures could conceivably result from attachment of Hg to Hg_2 $A0_g^{\pm}$, producing higher states of the trimer.

III. Attachment of Excited Mercury Atoms to Other Molecules

The Hg($^3P_0$) metastable mercury atoms will attach other molecules to form excited complexes which emit in the ultraviolet and visible spectral regions.

Several conditions have to be met; first, the bonding energy between $^3P_0$ and a ligand X has to be $\gg kT$; secondly, the collision complex has to be sufficiently long lived to allow for termolecular stabilization, i.e., removal of the excess vibrational energy; and thirdly, the potential energy surface of the stabilized complex must not cross that of the ground electronic state in the thermally accessible region. Some extreme examples would be atomic helium which is not significantly bound to the excited atom, H_2S for which the collision complex too rapidly fragments to give H plus SH, and CO which apparently is too strongly bound and crosses over to the ground electronic state.[32c] The $^3P_0$ plus CO complex, having the structure listed in Table II has the O^- representation, and formally the electric dipole transition to the ground state is forbidden; it should be weakly allowed, however, by rotation.

Conditions for the formation of stabilized complexes can be met for NH_3, amines, H_2O, alcohols and ethers.[33-39] A survey of the earlier work is given in ref 38.

At present, only four systems have subsequently been worked through in detail, with the spectra and kinetics adequately defined; these are complexes of $^3P_0$ with NH_3, *tert*-butylamine, diethylamine, and H_2O. Widely different behavior and variety are found even within this small group.

The following general mechanism will be applied.

$$Hg(^3P_0) + X \underset{k_{-1}}{\overset{k_1}{\rightleftharpoons}} HgX^{*+} \quad \text{(i)}$$

$$Hg\ X^{*+} \xrightarrow{k_2} Hg(^1S_0) + X + h\nu \quad \text{(ii)}$$

$$HgX^{*+} \xrightarrow{k_3} \text{nonradiative decay} \quad \text{(iii)}$$

$$HgX^{*+} + M \xrightarrow{k_4} HgX^* + M \quad \text{(iv)}$$

$$HgX^* \xrightarrow{k_5} Hg(^1S_0) + X + h\nu \quad \text{(v)}$$

$$HgX^* + X + M \rightleftharpoons HgX_2^* + M$$

The star superscript indicates electronic excitation, and the cross additional vibrational excitation. With NH_3 and H_2O, redissociation of HgX^{*+} to Hg($^3P_0$) plus X is its predominant fate. With the amines, the redissociation reaction has a negligible role; the greater density of vibrational states of the higher molecular weight complexes causes k_{-1} to be relatively small; with low amine pressures reaction iii becomes dominant, resulting in very low quantum yields for delayed emission, and removal of $^3P_0$ via a bimolecular reaction. It is only in the NH_3 system that the removal of $^3P_0$ has been shown to occur by termolecular kinetics, which predominantes at high pressures when reaction iv becomes the major channel for removal of HgX^{*+}.

We first give a summary of the research involving the Hg, NH_3 system. If mixtures of Hg vapor and NH_3 are excited with the 2537-Å resonance radiation, a very strong luminescence occurs in the ultraviolet at 3500 Å; the quantum yield is $\sim$0.7 in NH_3 alone, but increases to $\simeq$1.0 if an excess of N_2 is present. Although the emission was first observed many years ago,[40,41] the nature of its origin was only revealed comparatively recently when time-resolved techniques become available. Thus, with a phase-shift method,[33] the emission was shown to result from interaction of $^3P_0$ with NH_3, this was confirmed with the resonance flash method,[34] and it was further demonstrated that the removal of $^3P_0$ occurs with both bimolecular and termolecular reactions; the radiative lifetime of the complex has been reported to be $\simeq$1.8 μs.[36,38,45]

With low NH_3 pressures, <0.5 Torr, the mean lifetime of $^3P_0$ is greater than that of the $HgNH_3$* stabilized complex. With an initiating light flash of negligibly short duration, the time variation of the luminescence from the complex should approximate to a double exponential, the lifetime of the complex shaping the rise, and that of the $^3P_0$ the decay. Indistinguishable mean lifetimes, τ, for the $^3P_0$ decay and the sensitized luminescence decay have been demonstrated.[34]

Also, in the intermediate and low pressure regimes, the $HgNH_3^{*+}$ can be taken to be in equilibrium with free $^3P_0$ at low pressures, and the reciprocal mean lifetime of both $^3P_0$ and the $HgNH_3$* intensity, I, are given by

$$\tau^{-1} = -\frac{\mathrm{d}\ln[^3P_0]}{\mathrm{d}t} = -\frac{\mathrm{d}\ln I}{\mathrm{d}t} = \frac{k_1}{k_{-1}}[NH_3]\,[k_2 + k_3 + k_4[N_2]]$$

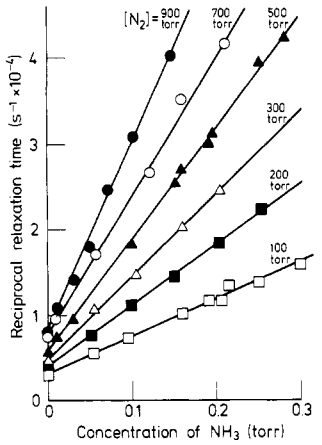

Figure 20. Relaxation of $Hg(^3P_0)$ by NH_3 with various $[N_2]$. [Hg] = 1.4 mtorr (300 K).

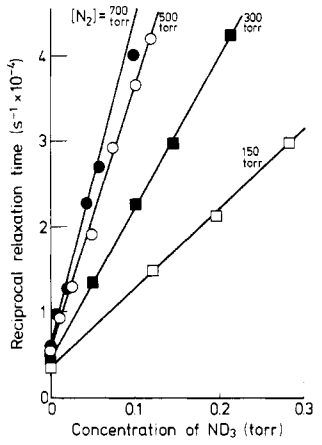

Figure 21. Relaxation of $Hg(^3P_0)$ by ND_3 with various $[N_2]$. [Hg] = 1.4 mtorr (300 K).

provided $[N_2] >> [NH_3]$. These quantities can therefore be derived from the appropriate ln plots.

Data for NH_3 and ND_3 are given in Figures 20 and 21; the dependence of the decay rate on both $[NH_3]$ and $[N_2]$ is well illustrated. From similar plots of τ^{-1} against $[N_2]$, the termolecular and bimolecular rate coefficients can be derived[42], the former reliably and accurately. We define $k_{ter} = k_1k_4/k_{-1}$.

The radiative lifetime of the stabilized complex can be measured using $[NH_3] \geq 20$ torr; the $^3P_0$ is then much shorter lived than the complex, the radiative lifetime of which then determines the decay profile of the luminescence.[42]

Measurements in NH_3 without added N_2 yield the most reliable value for the bimolecular component of the decay, $k_{bi} = k_1(k_2+k_3)/k_{-1}$, even though the system is complicated because of wall loss of $^3P_0$. The reciprocal relaxation time is then given by[43]

$$\tau^{-1} = D\alpha^2 + k_{bi}[NH_3] + k_{ter}[NH_3]^2$$

Here D is the $^3P_0$ diffusivity, and $a\alpha = 2.41$, where a is the reaction vessel radius. The 2.41 is the first root of the zeroth order Bessel function.

In Figure 22, $\tau^{-1}[NH_3]^{-1}$ is plotted vs. $[NH_3]$, shown by the filled points in the diagram. Subtraction of the $D\alpha^2/[NH_3]$ term gives the open points; the latter extrapolate back to give $k_{bi} = 1.1\ (\pm.2) \times 10^{-13}$ cm^3 molecule^{-1} s^{-1}, and $k_{ter}NH_3 = 2.6\ (\pm.3)$ t 10^{-30} cm^6 molecule^{-2} s^{-1} (293 K).

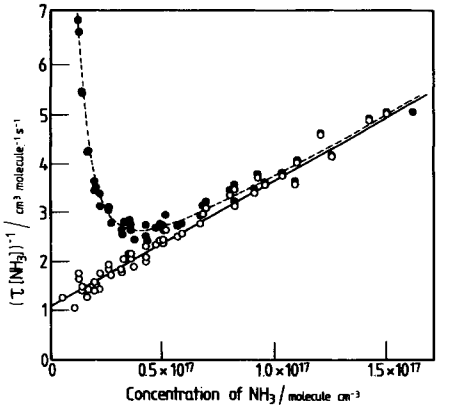

Figure 22. Variation of $[\tau NH_3]^{-1}$ with $[NH_3]$: ● experimental points; ○ after correction for wall loss.

TABLE IV. Termolecular Rate Coefficients for Formation of Excited Mercury Ammonia Complexes (cm^6 molecule^{-2} s^{-1})

	rate coef	ref
	NH_3 System	
$10^{30}k_{ter}^{NH_3}$	2.3 (±0.2)	44
	2.1 (±0.2)	42
	2.6 (±0.3)	43
$10^{31}k_{ter}^{N_2}$	2.1 (±0.2)	42
	1.88 (±0.02)	9
$10^{31}k_{ter}^{He}$	0.97 (±0.15)	43
	ND_3 System	
$10^{30}k_{ter}^{ND_3}$	3.41 (±0.20)	42
$10^{31}k_{ter}^{N_2}$	4.7 (±0.4)	42

Reported values of k_{ter} are listed in Table IV. Rate coefficients for the ND_3 system are significantly higher than for NH_3 by approximately 2-fold. This presumably implies that k_{-1} is smaller for the $HgND_3^{*+}$ complex, which may possibly be accounted for by a greater density of vibrational states in the deuteriated entity.

A minor disagreement still exits with regard to the decay rate of the stabilized complex with various $[NH_3]$; one group reports little variation[42] at up to 750 torr; the other gives a factor to two decrease of the $HgNH_3^*$ lifetime when the $[NH_3]$ is increased from 18 torr to 70 torr.[45]

The spectrum of the mercury ammonia luminescence is pressure dependent. An effect of increasing the $[NH_3]$ can easily be seen by eye, exciting an Hg, NH_3 mixture with light from a CW resonance lamp. With $[NH_3]$ at 10 torr, only faint violet emission is evident. The violet intensity increases with increasing $[NH_3]$ and appears blue at 1 atm. If the vessel is then warmed to increase the [Hg], the color of the luminescence turns to a bright apple green. The latter is referred to as the mercury ammonia green emission.

With $[NH_3]$ in the range 10^{-3} torr to 10 torr, with an excess of added N_2 or other inert gas, the diffuse emission band corresponds to the stabilized $HgNH_3^*$ monomer, shown in Figure 23, with an intensity maximum at 3450Å. It is also demonstrated in Figure 23 that if the $[NH_3]$ is reduced below 1.0 torr, without added inert gas, the spectrum undergoes a violet shift, with a threshold close to 2650 Å, corresponding to the full excitation energy of $^3P_0$.

The spectrum at 0.3 torr, shown in Figure 23, was originally supposed to be close to that of the $HgNH_3^{*+}$ unstabilized monomer, because bimolecular removal of $^3P_0$ is predominant at this pressure.[49] However, it turns

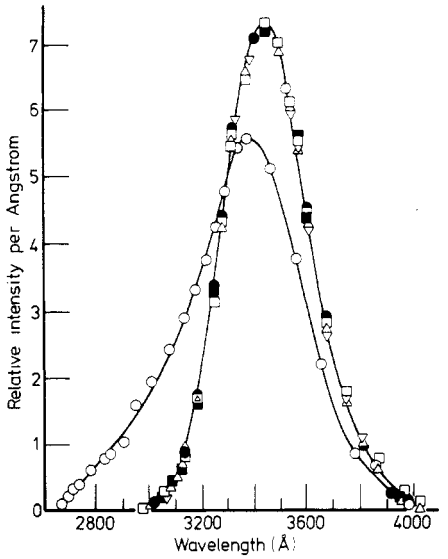

Figure 23. Ultraviolet emission of the excited mercury ammonia complex (295 K). ● $[NH_3]$ = 20 torr. Each of the following with 0.3 torr NH_3. △ $[N_2]$ = 600 torr; □ $[C_2H_6]$ = 600 torr; □ $[CF_4]$ = 600 torr; ▽ [Ar] = 600 torr; ○ no added gas.

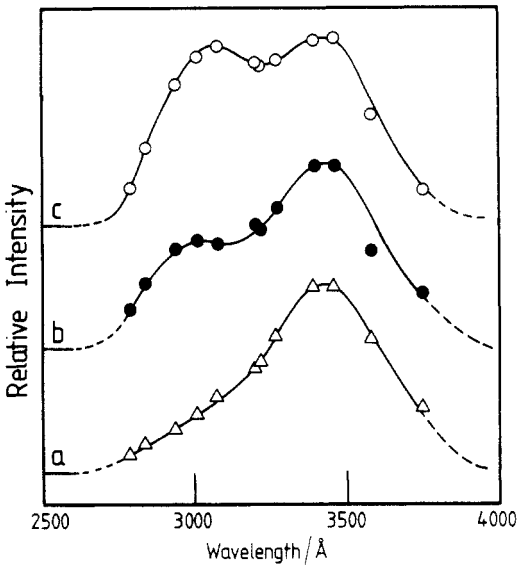

Figure 24. Variation of the emission spectrum of the excited mercury ammonia complex with $[NH_3]$ in the low-pressure regime. Spectra have been scaled to a common amplitude at 3460 Å and displaced for clarity of presentation. $[NH_3]$ in torr as follows: (a) 0.25, (b) 0.127, (c) 0.08.

out that the emission quantum yield of the unstabilized monomer is small, ~0.06, and it was subsequently reported that the spectrum continues to undergo a violet shift if the $[NH_3]$ is reduced below 0.3 torr.[46] It was concluded, furthermore, that in this low-pressure regime the luminescence is comprised of the superposition of two diffuse bands; one component is the stabilized monomer spectrum of Figure 23; the other is a band of similar Gaussian profile and width, but violet shifted with a maximum at 3000 Å. The upper electronic state of the short wavelength member was assigned to one of the electronic representations belonging to the $^3P_1$,NH_3 asymptote.[46]

These observations of the low-pressure spectrum were largely confirmed with the resonance flash method.[43] Examples of spectra down to 0.08 torr are given in Figure 24, and the resolved individual components in Figure 25, similar to those of ref 46. By time resolving

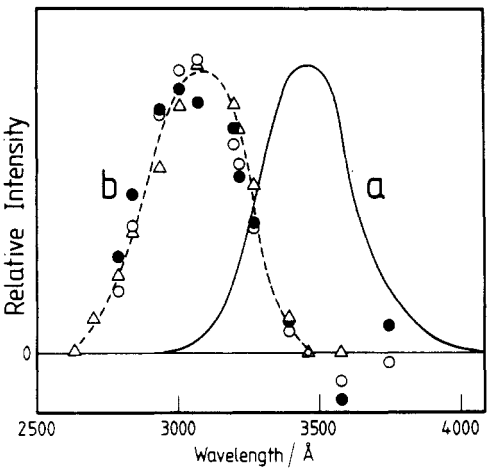

Figure 25. Representation of the low pressure mercury ammonia emission in terms of two components. "a" Upper state correlating with $^3P_0$. "b" Upper state correlating with $^3P_1$. The "a" spectrum is similar to that of the stabilized complex.

each of the diffuse bands, and from a variety of other kinetic aspects, it was concluded that the 3000-Å member arises solely from interaction of $^3P_0$ with NH_3, and that there is negligible emission due to direct interaction of $^3P_1$ with NH_3.[43] Other experiments, adding inert gas to reduce loss of $^3P_0$ to the walls, addition of scavengers to remove selectivity the long lived $^3P_0$, further established this mechanism[47] which is now generally accepted.[48]

The stabilized $HgNH_3$* correlates with the $^3P_0$,NH_3 asymptote, and has the A_2 representation; the electric dipole transition to the ground A_1 state is forbidden; it is, however, weakly allowed because of vibronic interactions. There are two states, A_1 and E, which correlate with the $^3P_1$,NH_3 asymptote; electric dipole transitions to the ground $^1S_0$,NH_3 state are both allowed. In the unstabilized $^3P_0$,NH_3 complex there is sufficient excess energy to populate the states which correlate with the $^3P_1$ asymptote, and they become statistically partitioned:

$$HgNH_3(A_2) \rightleftharpoons HgNH_3(A_1,E)$$

Because of the greater density of vibrational states accessible to the A_2 level, it must carry the major fraction of the excitation; but since the emission rates of the A_1, E states are greater, their role in the radiative decay of $HgNH_3{}^{*+}$ is about the same as that of the lower states.

The orders of magnitude of the various processes have been estimated[47] as follows:

$$^3P_0 + NH_3 \underset{2.5 \times 10^{10}}{\overset{2.5 \times 10^{-10}}{\rightleftharpoons}} HgNH_3{}^{*+}$$

$$HgNH_3{}^{*+} \xrightarrow{1.1 \times 10^7} \text{total spontaneous decay}$$

$$HgNH_3{}^{*+} \xrightarrow{7 \times 10^5} {}^1S_0 + NH_3 + h\nu$$

(units cm^3 $molecule^{-1}s^{-1}$ or s^{-1}). At sufficiently elevated temperatures a significant thermal population of the higher states should cause the 3000-Å band to appear even at high pressures. Presumably chemical decomposition of the NH_3 is responsible for the major part of the spontaneous decay of $HgNH_3{}^{*+}$.

As the $[NH_3]$ is raised above 10 torr in this system, the luminescence starts to undergo a red shift; these

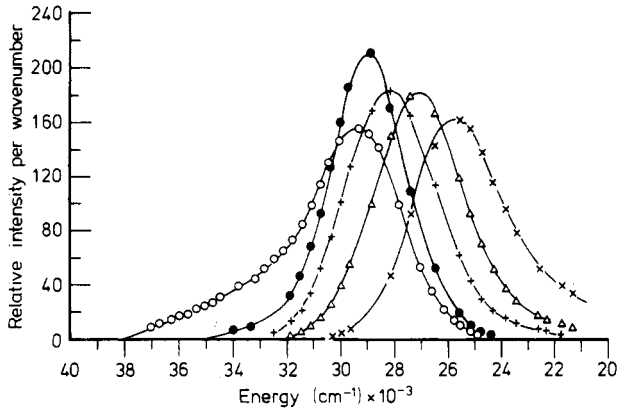

Figure 26. Observed spectra of the mercury ammonia emission, and their synthesis from individual profiles (295 K). $[NH_3]$ in torr as follows: ○, 0.3; ●, 20; +, 200; △, 937; ×, 5656. Full lines synthesized profiles.

TABLE V. Dissociation Constants for Mercury Ammonia Complexes and Estimates of the Total Binding Energy[49]

species	temp, K	dissociation const, molecule cm^{-3}	binding energy, kJ mol^{-1}
$Hg(NH_3)_2$*	295	6.2 (±.6) × 10^{18}	76
$Hg(NH_3)_2$*	404	7.5 (±2.5) × 10^{19}	76
$Hg(NH_3)_3$*	295	5.05 (±.7) × 10^{19}	86
$Hg(NH_3)_4$*	295	9.1 (±1.8) × 10^{19}	
$Hg(NH_3)_5$*	295	~2.2 × 10^{20}	
$Hg(NH_3)$*			50

spectral changes are due to attachment of additional molecules of NH_3 to $HgNH_3$*. Some sets of spectra, obtained with a cw technique,[49] are given in Figure 26, all normalized to a common area. An initial inspection of these data shows that with $[NH_3]$ at 937 torr there is very little emission from the $HgNH_3$* monomer; with 5656 torr the complex giving rise to the violet wing of the band with $[NH_3]$ at 937 torr is no longer present.

The various cluster species, $Hg(NH_3)_n$*, are in equilibrium in this system; each attachment causes a red shift, including a shift of the short wavelength threshold. Thus, for example, in the NH_3 pressure region up to 100 torr where the emitters are principally the monomer and dimer, analysis of the intensity just above the monomer threshold, as a function of $[NH_3]$, gives the fraction of the emission due to the monomer which can then be subtracted. By such repetitive and iterative procedures, profiles of dimer, trimer and tetramer have been defined, as well as the dissociation constants which determine the relative concentration. The individual spectra are shown in Figure 27, and the equilibrium constants in Table V. The lines drawn through the experimental points of Figure 26 are synthesized spectra using the individual spectra of Figure 27, and the dissociation constants in Table V. Successful analysis as described is possibly only if extremely accurate experimental profiles are obtained.

At 404 K, the pressure variation of the spectra was examined at up to 2 atm pressure; the effects of clustering are much less marked at the elevated temperature, and only monomer, dimer, and unstabilised emissions were observed.[49] No kinetic data have been derived above 300 K.

Recently, photoinduced association of $^1S_0$,NH_3 van der Waals molecules into the $HgNH_3A_2$ state has been demonstrated, exciting gas mixtures with dye laser radiation in the 2600–2680-Å region.[50] Electronic absorption spectra of the $Hg(NH_3)_n$* complexes have also been observed recently.[51]

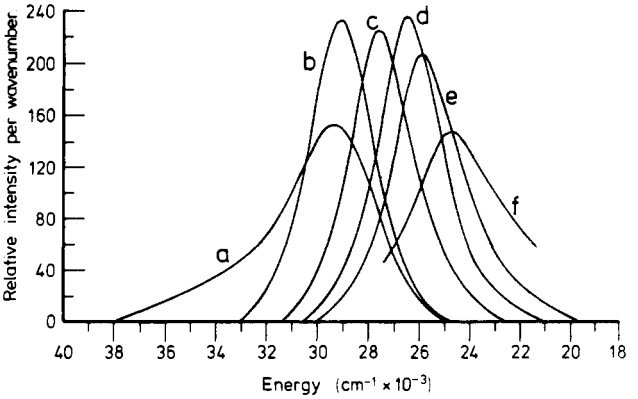

Figure 27. Emission spectra of $Hg(NH_3)_n$* complexes: (a) 0.3 torr spectrum, (b) stabilized monomer, (c) dimer, (d) trimer, (e) tetramer, (f) higher members.

We complete the section on the mercury ammonia luminescence with some brief comments on the green emission. It is known to arise in some way via mercury dimer formation from the stabilized $HgNH_3$*:[49]

$$HgNH_3^* + Hg(^1S_0) \rightarrow Hg_2\ A0_g^{\pm} + NH_3$$

The intensity increases with increasing [Hg], and if examined superficially might seem to be due to Hg_3* emission. The system has been examined at 780 K, with high [Hg] densities.[52] The mercury was excited using as the source XeI radiation, one band of which overlaps the 2537-Å line. The spectrum emitted by the excited gas was shown to be similar to the Hg_3* green emission in wavelength and profile, but distinctly narrower; substitution of ND_3 caused a small red shift. It was concluded that the carrier is Hg_2NH_3*, with a measured lifetime of 3.8 μs.

However, examination of this green emission at ambient temperature with the resonance flash method indicates a higher level of complexity,[53] with two emitting species, one peaking at ~4730 Å, and the other being very similar in profile and wavelength to the Hg_3* emission. The carrier of the former is possibly Hg_2NH_3*, because it increases in intensity, relative to the long wavelength band, with increasing NH_3 and decreasing [Hg]. The rate of the decay of the emission increases with both [Hg] and $[NH_3]$, but not linearly. With $[NH_3]$ = 1.2 torr and [Hg] = 2 × 10^{-3} torr, the mean lifetime of the emission is 10^{-4} s, decreasing to 0.6 × 10^{-4} s with $[NH_3]$ = 10 torr with the same [Hg]; in each case N_2 was added at 500 torr. The emitter of the long wavelength member could conceivably be Hg_3NH_3*. However, the kinetics of the rise and decay of the mercury ammonia green emission are complex and have not yet been analyzed.

These comments conclude the description of the mercury ammonia system, which has several remarkable and unique features.

We now turn our attention to the excited mercury water luminescence, which provides a simple contrast to the complex ammonia system. Quenching of $^3P_1$ by H_2O produces $^3P_0$ with unit quantum yield. With pulsed excitation, a delayed luminescence can be observed with the profile shown in Figure 28.[54] It may be noted that the diffuse spectrum is unaffected by variation of both $[H_2O]$ and added gas pressure. The

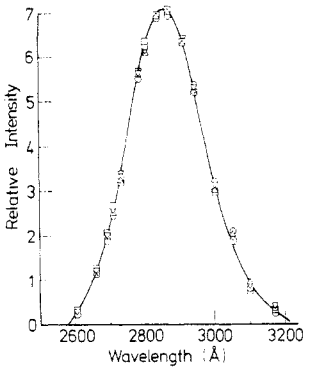

Figure 28. Ultraviolet emission in the $Hg(^3P_0)$ H_2O system (383 K). All pressures in torr: ○ $[H_2O]$ = 90, $[N_2]$ = 325; △ $[H_2O]$ = 250, $[N_2]$ = 725; ▽ $[H_2O]$ = 275, $[N_2]$ = 325; □ $[H_2O]$ = 600, $[N_2]$ = 325.

TABLE VI. Experimental Data for the Mercury Photosensitized Luminescence of Water Vapor[54]

temp, K	quantum yield	k_1, cm^3 molecule^{-1} s^{-1}	k_2, cm^3 molecule^{-1} s^{-1}
293	0.28 (±0.05)	1.5 (±0.2) × 10^{-15}	3.9 (1.0) × 10^{-15}
314	0.25 (±0.5)	1.4 (±0.25) × 10^{-15}	4.1 (1.5) × 10^{-15}
349	0.18 (±0.6)	1.31 (±0.2) × 10^{-15}	8.0 (3.0) × 10^{-15}

band is at a much shorter wavelength than that of $HgNH_3$*, and the violet wavelength threshold extends back to 2650 Å, or slightly below, corresponding to the $^3P_0$ excitation energy. Addition to the system of trace quantities of O_2 greatly reduces the luminescence whilst only slightly decreasing the 2537-Å emission intensity; evidently the band shown in Figure 28 is due to a $^3P_0$,H_2O complex. The same conclusion had previously been indicated with the phase shift method.[55,56]

However, the intensity of the luminescence in the mercury water system is proportional to $[^3P_0][H_2O]$, and independent of the total pressure.[54] This was established by observing relative intensities in mixed H_2O,NH_3 systems; increase of the total pressure increased the $HgNH_3$* intensity relative to that of HgH_2O*. From similar experiments, the quantum yields of the HgH_2O* emission were also recorded and are listed in Table VI.

The HgH_2O* emission band has a maximum at 2850 Å, well separated from the threshold (~0.33 eV). However, the observation of a distinct maximum to the red of the threshold does not establish that the $^3P_0$,H_2O interaction is attractive. At large separation the emission rate is, of course, zero, and the shape of the emission band will depend on the difference between the potential energy functions of the excited and ground states where the transition moment begins to be switched on by the H_2O,$^3P_0$ interaction. The complex with C_{2v} symmetry has the A_2 representation, and emission to the ground A_1 state is only weakly allowed because of vibronic interactions. The radiative lifetime is expected to be much longer than that of the $HgNH_3$* species, because the bonding of $^3P_0$ to H_2O is much weaker. A lifetime of the complex with high $[H_2O]$ has been derived from phase shift measurements;[55] however, the meaning of these experiments has been questioned because removal of $^3P_0$ by H_2O shows bimolecular kinetics with those conditions.[54]

The interaction potential of $^3P_0$ with H_2O obviously is attractive at long range, but with a well depth only of the order of kT at ambient temperature. Even if there is a termolecular component of the kinetics leading to weakly bound complexes, the associated relaxation time would be too short to observe with the resonance flash method because of the fast redissociation step:

$$Hg(^3P_0) + H_2O + M \rightleftharpoons HgH_2O^* + M$$

The reciprocal relaxation time for the establishment of equilibrium is the sum of the rates of the forward and backward steps; the latter would be expected to occur at about the gas kinetic collision rate. For the stabilized $HgNH_3$* complex, collisional redissociation to $^3P_0$ plus NH_3 does not significantly compete with spontaneous emission at ambient temperature, because the entity is too strongly bound.

In the $^3P_0$,H_2O system, therefore, the HgH_2O* very rapidly attains a statistical population relative to separated $^3P_0$ plus H_2O, and the decay of the excitation is first order in $[H_2O]$ and unaffected by adding excess Ar or N_2.

The kinetics of removal of $^3P_0$ can be expressed in terms of two bimolecular steps:

$$Hg(^3P_0) + H_2O \xrightarrow{k_1} Hg(^1S_0) + H_2O + h\nu$$

$$Hg(^3P_0) + H_2O \xrightarrow{k_2} \text{radiationless decay}$$

Some values of k_1 and k_2 are listed in Table VI.

The gross difference in behavior of the mercury ammonia and mercury water systems can be rationalized in terms of the ionization potentials of the ligands, which are respectively 10.15 eV and 12.6 eV. Water is less able to donate electrons to the vacant s orbital of the excited Hg atom.

The phase shift experiments provided general guidance with regard to the classes of substance which give rise to mercury photosensitized luminescence.[56] Thus it is shown that excited complexes of the primary amines with $^3P_0$ can be stabilized, and emit in a similar spectral region to $HgNH_3$*. Secondary and tertiary amines are shown to give comparatively very small or zero quantum yields of luminescence due to complexation with $^3P_0$.

With the resonance flash method, a single primary amine, *tert*-butylamine ($C(CH_3)_3NH_2$), has been examined in detail.[57] Considering the general, basic mechanism,

$$Hg(^3P_0) + A \underset{k_{-1}}{\overset{k_1}{\rightleftharpoons}} HgA^{*+} \text{ (A = amine)}$$

$$HgA^{*+} \xrightarrow{k_3} \text{nonradiative decay}$$

the mercury *tert*-butylamine differs from the NH_3 system in that $k_3 >> k_{-1}$, so that removal of $^3P_0$ by the amine is found to be bimolecular, to within the error limits.

Some emission spectra with high total pressures and with CW excitation are shown in Figure 29. In an excess of N_2 the profile of the emission is not significantly affected when the amine pressure is varied between 10^{-4} torr and 1 torr. This spectrum is due to the HgA*-stabilized monomer, curve "a" of Figure 29, and is similar to that of $HgNH_3$* but slightly red shifted, with a violet threshold at 3100 Å. With increasing amine pressure, however, a massive shift to the red

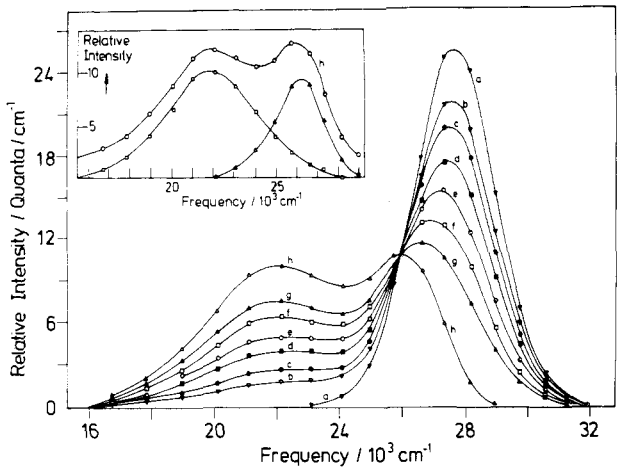

Figure 29. Variation of spectral profiles with pressure of *tert*-butylamine. (a) Stabilized monomer (h) dimer. Profiles "b", "c", "d", "e", "f", and "g" correspond to amine pressure of 17, 28, 46, 73, 120, and 189 torr, respectively. The inset illustrates a tentative analysis of the dimer spectrum into 2 bands.

occurs, a strong visible emission being easily detectable by eye.

The spectra of Figure 29 have been normalized to a common area, and when presented in this manner the profiles have an isosbestic common point of intersection. This is characteristic of the superposiiton of just two basic functions, which when normalized to a common area have the same amplitude at the isosbestic frequency. One function is the emission spectrum of the stabilized monomer, and the other that of the HgA_2* stabilized dimer. The addition of excess N_2 does not affect the spectra, and evidently monomer and dimer coexist in equilibrium:

$$HgA^* + A \rightleftharpoons HgA_2^*$$

With pulsed excitation they exhibit the same time variation.

Mathematical analysis of the spectra of Figure 29, to obtain the dimer spectrum, is straightforward (below 23 000 cm^{-1} there is no overlap) and is shown as profile *h*. It encompasses a wide frequency range, almost a factor of two, and its radiative decay must have access to two electronic systems, giving rise to two maxima. A tentative analysis of the dimer band into two Gaussian functions with maxima at 3810 Å and 4560 Å is shown in the inset to Figure 29. Presumably the upper state of the long wavelength member formally correlates with the $^3P_1$,A asymptote; the geometry of its equilibrium conformation has a high potential energy in the electronic ground state. This is illustrated schematically in Figure 30.

With low amine and total pressures, the spectrum shows a violet shift due to emission from the unstabilised monomer, HgA*$^+$; spectral profiles are given in Figure 31. The set of normalized spectra are again isosbestic, one component corresponding to the stabilized complex, and the other to the unstabilized, shown by function "*e*". The ratio of the intensity of the stabilized to the unstabilized spectrum is constant on the low frequency side, to within the error limits; this indicates that the broad unstabilized feature is a superposition of the profile similar to that of the stabilized monomer, with another band, the upper state of which correlates with $^3P_1$. A tentative analysis along these lines is included in the inset to Figure 31. The obser-

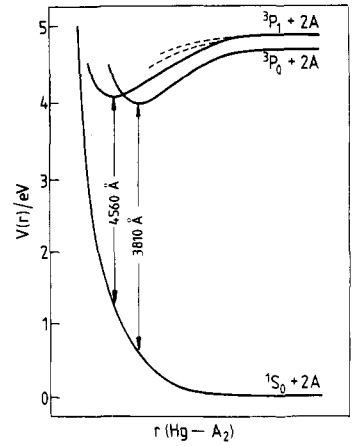

Figure 30. Schematic potential energy diagram of the excited mercury *tert*-butylamine dimer.

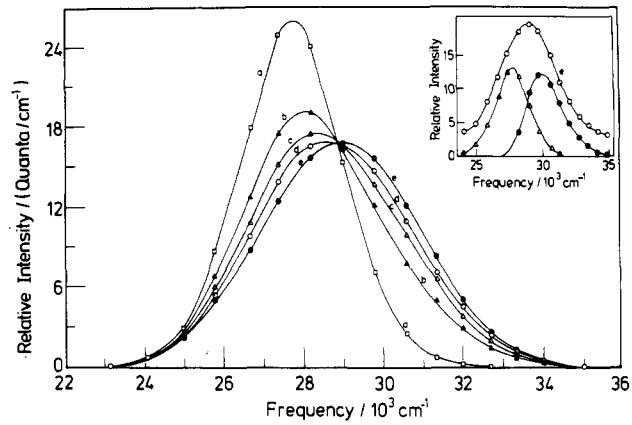

Figure 31. Violet shift of the luminescence with low pressures of *tert*-butylamine. (a) Stabilized monomer; (e) unstabilized monomer. In "b", "c", and "d" the amine pressures are 0.15, 0.061, and 0.03 torr, respectively. The inset shows a tentative analysis of the unstabilized spectrum into 2 bands.

vation of emission from the unstabilized monomer is similar to the ammonia system, though the latter spectrum exhibits two maxima (Figure 24): the HgA*$^+$ has sufficient energy to access higher electronic states.

The oscilloscope traces of Figure 32 illustrate the kinetic investigations of the spectral assignments. The first aspect concerns the low-pressure emission. With 5 torr of amine the relaxation times for both $^3P_1$ and $^3P_0$ are small compared with the flash duration; therefore the unstabilized component should follow the flash profile, whilst that of the stabilized component should be delayed because of its finite radiative lifetime. These points are demonstrated in "a" and "b". In "a" the spectrometer is set at 3060 Å and in "b" at 3550 Å. The radiative lifetime of the stabilized monomer is found to be 2.1 μs.

If the high frequency component of the low-pressure emission is due to complexation of $^3P_0$ with the amine, then at very low pressure it should be delayed relative to the exciting flash. This is shown to be the case in "c" of Figure 32, observing emission at 3060 Å with 0.2 torr of amine, plus 30 torr of N_2 to induce the $^3P_{1\rightarrow0}$ relaxation. In "d" the spectrometer was set at 3550Å, the stabilized monomer region; the decay time is indistinguishable from trace "c".

The experiments illustrated in "e" and "f" demonstrate that the relaxation times of the stabilized monomer and dimer are indistinguishable. The rate coefficient for bimolecular removal of $^3P_0$ by *tert*-bu-

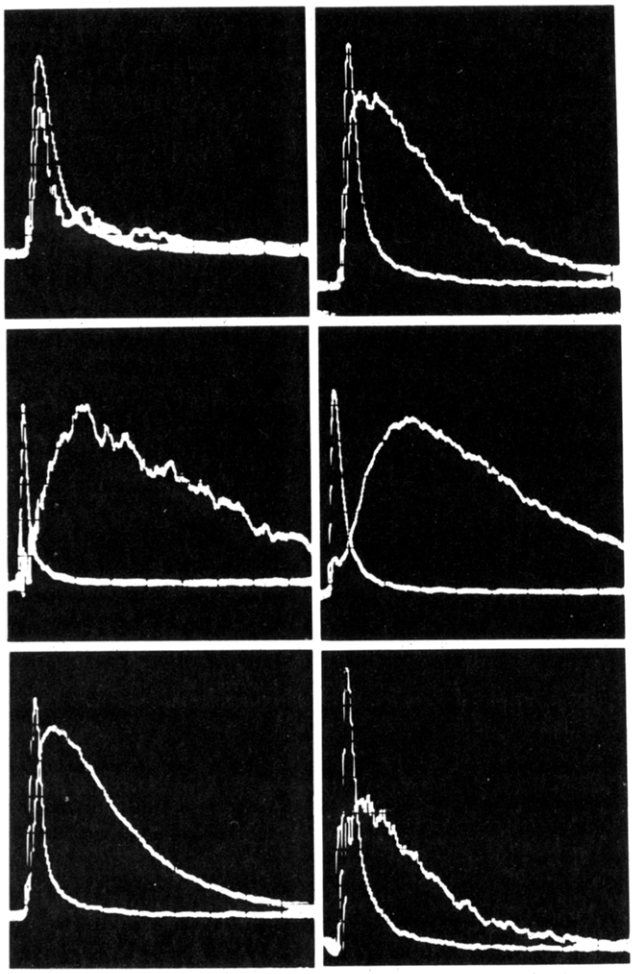

Figure 32. Time-resolved profiles of the Hg($^3P_0$] *tert*-butylamine emission with various pressures and wavelengths (295 K). Each of the smooth short traces is the flash profile. Top left, 5 torr amine, 3060 Å, 10 μs full scale; top right, 5 torr amine, 3550 Å, 10 μs full scale; middle left, 10^{-2} torr amine, 3060 Å, 20 μs full scale; middle right, 10^{-2} torr amine, 3550 Å, 20 μs full scale; bottom left, 10 torr amine, 3550 Å, 10 μs full scale; bottom right, 10 torr amine, 4500 Å, 10 μs full scale.

tylamine was recorded at 4.0 (±.5) × 10^{-10} cm^3 $molecule^{-1}$ s^{-1} at 295 K.

Although the addition of Ar or N_2 does not affect the time behavior of the Hg photosensitized luminescence of *tert*-butylamine, both gases enhance the intensity because they increase the quantum yield of formation of the stabilized complex. The half-pressure for stabilization by Ar is 47 (±7) torr, whilst that of the parent is13.8 (±1.4) torr. Results for this system are listed in Table VII.

The origin of the main differences between the ammonia and *tert*-butylamine kinetic systems can be understood quite simply by examining the k_{-1} and k_3 values, and their ratios:

$$^3P_0 + NH_3 \xleftarrow{10^{10}\ s^{-1}} HgNH_3{}^{*+} \xrightarrow{2\times10^7\ s^{-1}} \text{spontaneous decay}$$

$$^3P_0 + A \xleftarrow{3\times10^7\ s^{-1}} HgA^{*+} \xrightarrow{2\times10^8\ s^{-1}} \text{spontaneous decay}$$

For the NH_3 system, k_{-1}/k_3 is large and the kinetics exhibit a termolecular component for $^3P_0$ removal. The k_{-1}/k_3 is very small for the *tert*-butylamine case, and hence there is negligible termolecular removal of $^3P_0$;

TABLE VII. Kinetic Data for the Hg* *tert*-Butylamine System (295 K)

The Stabilized Monomer	
emmission quantum yield	1.0 (±0.1)
emmission rate	4.8 (±0.3) × 10^5 s^{-1}
The Unstabilized Monomer	
spontaneous decay rate	~2 × 10^{18} s^{-1}
spontaneous emission rate	2.6 × 10^6 s^{-1}
Formation of $^3P_0$ from $^3P_1$	
quantum yield	~0.38
Removal of $^3P_0$	
bimolecular rate coefficient	4.0 (±.5) × 10^{-10} cm^3 $molecule^{-1}$ s^{-1}
termolecular rate	not detected

because the HgA* has a much higher emission quantum yield than the unstabilized complex, the phenomenon of collisionally induced enhancement of the luminescence intensity is found.

The k_{-1} is relatively small for the *tert*-butylamine unstabilized complex because the large molecule has a high density of states at that energy. The k_3 for *tert*-butylamine is higher than that for the NH_3 system because channels for chemical decomposition are more exothermic.

In an attempt to broaden further the scope for molecular attachment to the excited mercury atom, we have considered the possibility of preparing the excited complexes by ligand exchange with $HgNH_3$*, viz.,

$$HgNH_3{}^* + X \rightarrow HgX^* + NH_3$$

Thereby the energy of the nascent HgX^{*+} is reduced, to render less accessible channels leading to chemical decomposition. The general scheme has been demonstrated for the diethylamine ligand.[39]

The secondary amine, at various pressures, was irradiated with 2537 Å cw radiation in the presence of Hg vapour at 293 K; no luminescence was detected, in accord with a previous report.[56]

Preliminary experiments were conducted with NH_3 pressures of ~1 atm, to attach the $^3P_0$ to the NH_3 in ~10^{-9} s; the amine can then be added up to 100 torr without catastrophic loss of excited atoms because of their direct removal by the amine. Addition of amine to the NH_3 induces a massive shift of the spectrum into the visible region, shown in Figure 33. The sets of normalized spectra are isosbestic, corresponding to the superposition of just two basic functions. The two carriers are the stabilized $Hg(Et_2NH)$* monomer and the $Hg(Et_2NH)_2$* dimer.

The monomer spectrum, with a maximum at 3700 Å, has a similar Gaussian profile to those of the ammonia- and *tert*-butylamine stabilized complexes. The emission spectrum of the $Hg(Et_2NH)_2$* dimer, Figure 34, however, lies much further to the red than any of the spectra discussed previously; it is believed to represent the superposition of emission from two electronic states, i.e., from a system with two potential minima, as found also for the *tert*-butylamine complex. However, for $Hg(Et_2NH)_2$* the long wavelength component of the dimer emission, with a maximum at 5140 Å, predominates.

The sequential NH_3 attachment and subsequent ligand exchange was time resolved, as shown in Figure 35. At 3200 Å, below the short wavelength threshold of the $Hg(Et_2NH)$* band, the emission due to $Hg(NH_3)$* is prompt and decays rapidly; at 4080 Å, above the Hg-

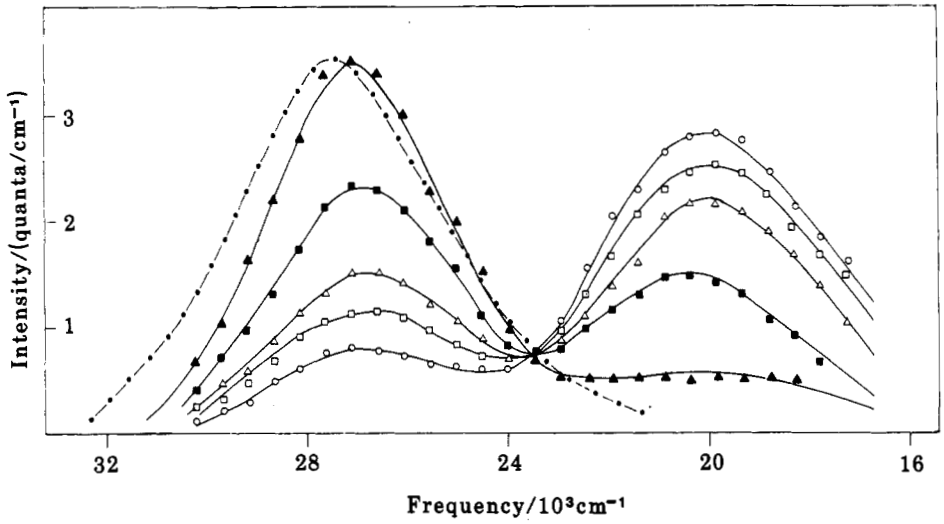

Figure 33. Excited mercury diethylamine spectra with $[NH_3]$ = 590 torr (295 K). Pressures in torr. ▲, 4.2 amine; ■, 20 amine; △, 44 amine; □, 68 amine; ○, 117 amine; ·–·, zero amine.

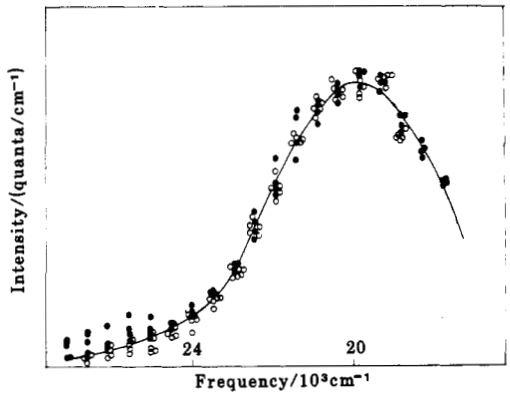

Figure 34. Emission spectrum of the $Hg(Et_2NH)_2$* complex: ●, 590 torr NH_3; ○, 250 torr NH_3.

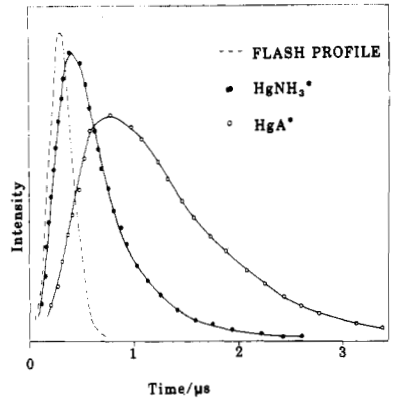

Figure 35. Time resolution of the ligand exchange reaction (295 K). Amine pressure 0.08 torr, $[NH_3]$ at 10 torr, 780 torr N_2. ---, flash profile at 2537 Å. ●, $Hg[NH_3]$* profile recorded at 3200 Å. ○, $Hg(Et_2NH)$* profile at 4080 Å.

(NH_3)* long wavelength threshold, emission due to $Hg(Et_2NH)$* decays comparatively slowly. The rate coefficient for ligand exchange

$$Hg(NH_3)^* + Et_2NH \rightarrow Hg(Et_2NH)^* + NH_3$$

is shown to be 2×10^{-10} cm^3 molecule^{-1} s^{-1} (293 K). The equilibrium constant of the above reaction is ~40, and clearly the Et_2NH complex is the more strongly bound. The lifetime of the stabilized monomer is 1.1×10^{-6} s.

With small partial pressures of Et_2NH in an excess of N_2, a very weak emission due to attachment to $^3P_0$ was finally observed in the afterglow following pulsed excitation; the emission quantum yield is 0.003 with $[N_2]$ = 400 torr. From these data the rate of spontaneous, radiationless decay has been estimated:

$$Hg(Et_2NH)^{*+} \xrightarrow[10^{11}\ s^{-1}]{} \text{spontaneous decay}$$

The scheme for preparation of $Hg(Et_2N)$* by ligand exchange greatly increases the emission yield because the nascent complex prepared by displacement of ammonia has less excess vibrational energy and therefore a comparatively small nonradiative decay rate: the energy of the excited atom is reduced stepwise.

Similar experiment with small pressures of trimethylamine, in excess NH_3, have demonstrated that the former will also attach to $^3P_0$ by ligand exchange, again causing a large red shift of the emission spectrum. This system has not been worked through in detail.

Excited complexes of $^3P_0$ with the aliphatic alcohols emit broad bands in the ultraviolet region.[54,55], with $2850 < \lambda_{max} < 3100$ Å. The alcohols are less strongly bound than the amines, and there is no evidence for termolecular removal of $^3P_0$ in these systems. The relaxation times for establishment of the equilibria,

$$^3P_0 + ROH + M \rightleftharpoons Hg(ROH)^* + M$$

are expected to be very short because the rate coefficient for the dissociation step will be large. There is evidence for clustering attachment of CH_3OH to $^3P_0$.[58]

The aliphatic ethers also luminescence in the presence of excited mercury atoms, in the same wavelength region as the alcohols.[37,39] With the monoethers, for example, diethyl ether, the intensity is extremely weak. For the diethers such as dioxane, and higher polyethers like trimethyl phosphate, the luminescence is of com-

TABLE VIII. Dissociation Energies (cm^{-1}) and Equilibrium Nuclear Separations (Å) of Rare Gas Mercury Complexes[60]

		HgNe	HgAr	HgKr
X^10^+	Do	42	131	168
	Re	3.87	4.01	4.07
A^30^+	Do	105	349	517
	Re	3.12	3.38	3.52
B^31	Do	13	61	90
	Re	4.57	4.66	4.57

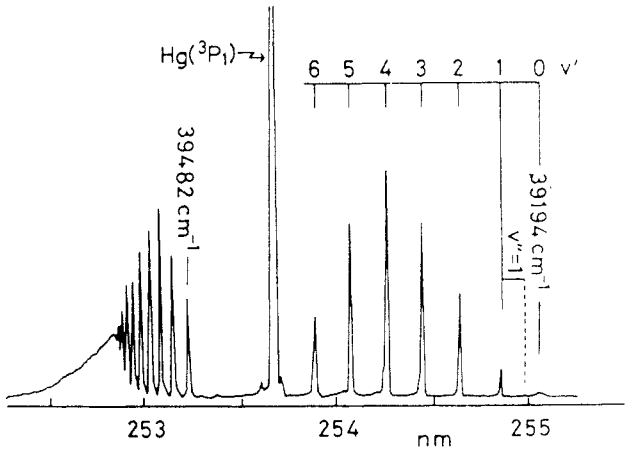

Figure 36. Dye laser excitation of the HgArA^{3}0$^+$ and HgArB^{3}1 states, respectively, to the red and blue of the resonance line. Reproduced with permission from ref 60. Copyright 1984, American Institute of Physics.

parable intensity to the alcohols. The crown ethers, for example 12-crown-4, appear to attach strongly. However, none of the alcohol or ether systems has been examined in detail.

Recently there has been considerable progress in understanding the structure of complexes of $^3P_1$ with the rare gases.[60] The van der Waals ground-state molecules, Hg–RG, were prepared in a supersonic jet and fluorescence spectra close to the 2537-Å line were excited with light from a pulsed dye laser. The laser excited two electronic systems, A^{3}0$^+$ → X^{1}0$^+$. and B^{3}1 → X^{1}0$^+$, both upper states belonging of course to the $^3P_1$–RG asymptote. (The usual convention in these Hund's case "c" states is to include the spin multiplicity in the representation, which we follow to avoid conflict.) Because of the cooling accompanying the nozzle expansion, the vibrational structures of the two systems are beautifully revealed, for Ne, Ar, and Kr complexes. The derived dissociation energies and equilibrium nuclear separations are listed in Table VIII. The Hg–Ar spectrum is shown in Figure 36.

The results of Table VIII show that in collision with a rare gas atom, the three wave functions of $^3P_1$ give rise to two molecular states; each of the A^{3}0$^+$ states is more strongly bound than the van der Waals states, with smaller equilibrium nuclear separations. On the contrary, the B^{3}1 states are even less strongly bound than the ground states, with larger nuclear separations. A qualitative explanation of these differnces can be seen using the orbital approximation, as follows.

Very simply, the basic characteristic is that occupancy of the pσ orbital of the mercury atom gives rise to repulsion of a rare gas atom at intermediate range. Thus the Hg–RG complexes are more strongly bound than the ground electronic state only if the atomic wave functions have zero pσ occupancy. Of the nine wave functions of a ^3P state, just three fulfil this condition; these are the $J = 1$, $M_J = 0$ state and the $J = 2$, $M_J = \pm 2$ states. The former combine with a rare gas atom to form the A^{3}0$^+$ states listed in Table VIII. In the $J = 1$, $M_J = \pm 1$ states the pσ and pπ orbitals are occupied with equal probability, and repulsion of the rare gas atom occurs at intermediate range; the corresponding degenerate B^{3}1 states are less strongly bound than the van der Waals states as shown in Table VIII, with large equilibrium nuclear separations. The results of Figure 8 constitute a substantial advance in this field, and also point the way ahead with regard to structure evaluation of the larger mercury complexes.

The Hg–Xe complexes of $^3P_1$ have not yet been studied with the molecular beam technique. However, they have been studied in thermal systems. Emission from HgXe A^{3}0$^+$ is quite strong when HgXe mixtures are excited at 2537 Å in a thermal system at ambient temperature. The A → X system is continuous with these conditions, having a maximum intensity at 2650 Å, well separated from the exciting line. From studies of the temperature variation of the spectral profile, the A state dissociation energy has been shown to be ~1400 cm^{-1}, with an equilibrium nuclear separation of 3.1 Å.[61,62] It is much more strongly bound than the other rare gas $^3P_1$ complexes. Emission from the HgXe B^{3}1 state has not been observed;[61] the B → X system probably has the appearance of a linelike feature close to the 2537-Å transition.

Attachment of the $^3P_2$ state of mercury to xenon has been described recently.[3] The $^3P_2$ can be prepared in xenon by exciting the $^1P_1$ state, which undergoes some degree of collisional deactivation:

$$^1P_1 + Xe \rightarrow {}^3P_2 + Xe$$

$$\text{rate coefficient} = 4 \times 10^{-12}\ \text{cm}^3\ \text{molecule}^{-1}\ \text{s}^{-1}$$

The $^3P_2$ does not undergo any significant deactivation to the lower J states in collision with xenon, and mean lifetimes of up to 600 μs have been observed with [Xe] = 760 torr.

When $^3P_2$ is prepared in xenon, two emission bands occur. One is a sharp feature, full width at half maximum ~446 cm^{-1}, the upper state of which has been assigned as HgXeD^{1}1; the corresponding atomic states are $J = 2$, $M_J = \pm 1$ for which the pσ and pπ orbitals are equally occupied: hence the complex is repulsive at intermediate range. The centroid of the emission is blue shifted from the $^3P_2 \rightarrow {}^1S_0$ forbidden line at 2270 Å, because the ground state is slightly more strongly bound than the upper state over the range of nuclear separations encompassed by the turning points of bimolecular collisions. The feature is narrow because both upper state and lower state potential energies vary little within this range of nuclear separation.

The other emission band which is observed in the $^3P_2$,Xe system is a broad feature which results from the formation of the bound HgXe C^{3}2 complex, the corresponding atomic states being $J = 2$, $M_J = \pm 2$ with zero pσ occupancy. The equilibrium constant for the reaction,

$$^3P_2 + Xe = HgXe\ C^32$$

has been recorded as 1.09 (±10.1) × 10^{-19} cm^3 molecule^{-1} s^{-1} at 293 K; correspondingly, with [Xe] at 760 torr some 73% of the $^3P_2$ is attached to Xe. The C^{3}2 dissociation energy is ~1700 cm^{-1}. However, from an analysis of the kinetics it has been shown that the carrier of the broad band is not HgXe C^{3}2 itself, but an HgXe$_2$(^{3}2$_u$) triatomic species; in a bent conformation, one component of the latter has B symmetry and can radiate to the A_1 ground electronic state.

Outstandingly interesting molecular beam experiments on the excited Hg,N$_2$ and Hg,H$_2$ systems have also been described recently. For the Hg,N$_2$ system,[11a] fluorescence was observed from an electronically excited

complex when the van der Waals molecule, cooled by nozzle expansion, was excited both to the blue and to the red of the 2537-Å line. The upper state of the complex, excited to the red, is expected to correlate with the $J = 1$, $M_J = 0$ state of the free atom. For the RG complexes these states have $^3O^+$ symmetry. The HgN_2 complexes should have C_{2v} symmetry (see Table II), in which case the complex has A_1 symmetry.

The upper states excited to the blue of the resonance line correlate with $J = 1$, $M_J = \pm 1$ and have B symmetry. The lifetime of these states was recorded as 100 ns, close to the radiative lifetime of $^3P_1$. The emission from the excited A_1 state exhibits beautifully resolved vibrational structure, indicative of both stretching and bending modes. It is also demonstrated that the lifetime of the complex decreases with increasing vibrational and rotational energy. By using a second laser to pump $^3P_0$ to 7^3S_1, the former was shown to be the reaction product.

$$HgN_2^*(A_1) \rightarrow {}^3P_0 + N_2$$

When the HgH_2 van der Waals complex was laser-excited close to the 2537-Å line, no fluorescence was detected; in this case the decomposition of the complex must occur much more rapidly than its spontaneous emission rate. The formation of rotationally hot HgH was detected by use of a second tunable laser.[63]

These comments complete an overview of the spectroscopy and kinetics of molecular attachment to Hg6s6p(^{3}P). The ability of the excited atom to form stable clusters with large organic entities is unique within molecular science. Specially intriguing has been to discover that whilst the mono-amine complexes emit a single band of Gaussian profile in the ultraviolet, addition of a second ligand gives rise to an emission band in the visible spectrum, in addition to an ultraviolet component slightly red shifted from that of the monomer. High-resolution spectra will eventually reveal what the equilibrium structures are at the potential minima, and how the ligands are oriented relative to each other.

Registry No. Hg, 7439-97-6; Hg_2, 12596-25-7; Hg_3, 11062-37-6.

References

(1) King, G. C.; Adams, A. *J. Phys. B* **1974**, *B7*, 1712.
(2) Bousquet, C.; Bras, N. *J. Phys.* (Les Ulis, Fr.) **1980**, *41*, 19.
(3) Callear, A. B.; Du, K. *Chem. Phys. Lett.* **1985**, *113*, 554; **1986**, *128*, 141.
(4) Calvert, J. G.; Pitts, J. N., Jr. *Photochemistry*; Wiley: New York, NY, 1966. Breckenridge, W. H. In *Reaction of Small Transient Species*; Fontijn, A., Clyne, M. A. A., Eds.; Academic: London, 1983.
(5) (a) Cvetanović, R. J.; *Progr. React. Kinet.* **1964**, *2*, 39. (b) Gleditsch, S. D.; Michael, J. V. *J. Phys. Chem.* **1975**, *79*, 409.
(6) Callear, A. B.; Kendall, D. R. *Chem. Phys.*, **1981**, *57*, 65.
(7) Hikida, T.; Santoku, M.; Mori, Y. *Rev. Sci. Instrum.* **1980**, *51*, 1063.
(8) Vikis, A. C.; Torrie, G.; Le Roy, D. J. *Can. J. Chem.* **1972**, *50*, 176.
(9) Callear, A. B.; McGurk, J. C. *J. Chem. Soc., Faraday Trans. 2* **1973**, *69*, 97.
(10) Callear, A. B.; Wood, P. M. *Trans. Faraday Soc.* **1971**, *67*, 272. Breckenridge, W. H.; Callear, A. B. *Trans. Faraday Soc.* **1971**, *67*, 2009. Callear, A. B. *Physical Chemistry*; Academic: New York, San Francisco, London, 1975, Vol. VIB.
(11) (a) Jouvet, C.; Soep, B. *J. Chem. Phys.* **1984**, *80*, 2229. (b) Freeman, C. G.; McEwan, M. J.; Claridge, R. F. C.; Phillips, L. F. *Trans. Faraday Soc.* **1971**, *67*, 2004.
(12) Horiguchi, H.; Tsuchiya, S. *Bull. Chem. Soc. Jpn.* **1971**, *44*, 3221.
(13) Callear, A. B.; McGurk, J. C. *J. Chem. Soc., Faraday Trans 2* **1972**, *68*, 289.
(14) Djeu, N.; Burnham, R. *Appl. Phys. Lett.* **1974**, *25*, 350.
(15) (a) Holmes, N. C.; Siegman, A. E. *J. Appl. Phys.* **1978**, *49*, 3155. (b) Krause, H. F.; Datz, S.; Johnson, S. G. *J. Chem. Phys.* **1973**, *58*, 367.
(16) Gover, T. A.; Bryant, H. G., Jr. *J. Phys. Chem.* **1966**, *70*, 2070.
(17) Granzow, A.; Hoffman, M. Z.; Lichtin, N. N. *J. Phys. Chem.* **1969**, *73*, 4289.
(18) Madhavan, V.; Lichtin, N. N.; Hoffman, M. Z. *J. Phys. Chem.* **1973**, *77*, 875.
(19) Hay, P. J.; Dunning, T. H., Jr.; Raffenetti, R. C. *J. Chem. Phys.* **1976**, *65*, 2679.
(20) Mies, F. H.; Stevens, W. J.; Krauss, M. *J. Mol. Spectrosc.* **1978**, *72*, 303.
(21) Stock, M.; Smith, E. W.; Drullinger, R. E.; Hessel, M. M. *J. Chem. Phys.* **1978**, *68*, 4167.
(22) Smith, E. W.; Drullinger, R. E.; Hessel, M. M.; Cooper, J. *J. Chem. Phys.* **1977**, *66*, 5667.
(23) Stock, M.; Smith, E. W.; Drullinger, R. E.; Hessel, M. M.; Pourcin, J. *J. Chem. Phys.* **1978**, *68*, 1785.
(24) Callear, A. B.; Lai, K.-L. *Chem. Phys. Lett.* **1980**, *75*, 234.
(25) Callear, A. B.; Lai, K.-L. *Chem. Phys.* **1982**, *69*, 1.
(26) Takeyama, H. *J. Sci. Hiroshima Univ. Ser. A: Math, Phys., Chem.* **1952**, *A15*, 235.
(27) Mrozowski, S. *Phys. Rev.* **1949**, *76*, 1714.
(28) Callear, A. B.; Kendall, D. R. *Chem. Phys. Lett.* **1979**, *64*, 401.
(29) Callear, A. B.; Devonport, C. P.; Kendall, D. R. *Chem. Phys.* **1981**, *61*, 65.
(30) Callear, A. B.; Kendall, D. R. *Chem. Phys. Lett.* **1980**, *70*, 215.
(31) Callear, A. B.; Kendall, D. R.; Devonport, C. P. *J. Chem. Soc., Faraday Trans. 2* **1982**, *78*, 1451.
(32) (a) Niefer, R.; Atkinson, J. B.; Krause, L. *J. Phys. B* **1983**, *16*, 3531, 3767. (b) Celestino, K. C.; Ermler, W. C. *J. Chem. Phys.* **1984**, *81*, 1872. (c) Kato, S.; Jaffe, R. L.; Komornicki, A.; Morokuma, K. *J. Chem. Phys.* **1983**, *78*, 4567.
(33) Freeman, C. G.; McEwan, J. M.; Claridge, R. F. C.; Phillips, L. F. *Chem. Phys. Lett.* **1970**, *5*, 555.
(34) Callear, A. B.; McGurk, J. *Chem. Phys. Lett.* **1972**, *7*, 491.
(35) Newman, R. H.; Freeman, C. G.; McEwan, M. J.; Claridge, R. F. C.; Phillips, L. F. *Trans. Faraday Soc.* **1970**, *66*, 2827, 2974.
(36) Koskikallio, J.; Callear, A. B.; Connor, J. H. *Chem. Phys. Lett.* **1971**, *8*, 467.
(37) Strausz, O. P.; Campbell, J. M.; De Paoli, S.; Sandhu, H. S.; Gunning, H. E. *J. Am. Chem. Soc.* **1973**, *95*, 732.
(38) Phillips, L. F. *Acc. Chem. Res.* **1974**, *7*, 135. Freeman, C. G.; Claridge, R. F. C.; McEwan, M. J.; Phillips, L. F. *Chem. Phys. Lett.* **1971**, *9*, 578.
(39) Callear, A. B.; Devonport, C. P. *J. Chem. Phys.* **1983**, *78*, 3738.
(40) Mitchell, A. C. G.; Dickinson, R. G. *J. Am. Chem. Soc.* **1927**, *49*, 1478.
(41) Gaviola, E.; Wood, R. W. *Phil. Mag.* **1928**, *6*, 1191.
(42) Callear, A. B.; Koskikallio, J.; Connor, J. H. *J. Chem. Soc. Faraday Trans. 2* **1974**, *70*, 1542.
(43) Callear, A. B.; Freeman, C. G. *Chem. Phys.* **1977**, *23*, 343.
(44) Freeman, C. G.; McEwan, M. J.; Claridge, R. F. C.; Phillips, L. F. *Trans. Faraday Soc.* **1971**, *67*, 2004.
(45) Hikida, T.; Santoku, M.; Mori, Y. *Chem. Phys. Lett.* **1978**, *55*, 280.
(46) Hikida, T.; Ichimura, T.; Mori, Y. *Chem. Phys. Lett.* **1974**, *27*, 548.
(47) Callear, A. B.; Kendall, D. R. *Chem. Phys. Lett.* **1978**, *58*, 31.
(48) Umemoto, H.; Tsunashima, S.; Sato, S. *Chem. Phys.* **1978**, *35*, 103.
(49) Callear, A. B.; Connor, J. H. *J. Chem. Soc., Faraday Trans. 2* **1974**, *70*, 1667.
(50) Horiguchi, H.; Tsuchiya, S. *Chem. Phys. Lett.* **1984**, *109*, 250.
(51) Hunziker, H. E., private communication, 1985.
(52) Mandl, A.; Hyman, H. A. *J. Chem. Phys.* **1981**, *74*, 3167.
(53) Callear, A. B., unpublished results.
(54) Callear, A. B.; Connor, J. H. *J. Chem. Soc., Faraday Trans. 2* **1974**, *70*, 1767.
(55) Freeman, C. G.; McEwan, M. J.; Claridge, R. F. C.; Phillips, L. F. *Trans. Faraday Soc.* **1971**, *67*, 2567.
(56) Newman, R. H.; Freeman, C. G.; McEwan, M. J.; Claridge, R. F. C.; Phillips, L. F. *J. Chem. Soc., Faraday Trans. 2* **1971**, *67*, 1360.
(57) Callear, A. B.; Kendall, D. R.; Krause, L. *Chem. Phys.* **1978**, *29*, 415.
(58) Luther, K.; Wendt, H. R.; Hunziker, H. E. *Chem. Phys. Lett.* **1975**, *33*, 146.
(59) Callear, A. B.; Devonport, C. P., unpublished results.
(60) Fuke, K.; Saito, T.; Kaya, K. *J. Chem. Phys.* **1984**, *81*, 2591.
(61) Lam, L. K.; Gallagher, A.; Drullinger, R. *J. Chem. Phys.* **1978**, *68*, 4411.
(62) Grycuk, T.; Findeisen, M. *J. Phys. B* **1983**, *B16*, 975.
(63) Breckenridge, W. H.; Jouvet, C.; Soep, B. *J. Chem. Phys.* **1986**, *84*, 1443.